Straggling in Energy Loss of Swift Hydrogen and Helium Ions in Gases

By F. BESENBACHER, H. H. ANDERSEN,
P. HVELPLUND, *and* H. KNUDSEN

Det Kongelige Danske Videnskabernes Selskab
Matematisk-fysiske Meddelelser **40**:9

Kommissionær: Munksgaard
København 1981

Synopsis

Straggling in energy loss for 40-keV to 1-MeV hydrogen ions and 100-keV to 2.4-MeV helium ions in a variety of atomic and molecular gases has been measured with an accuracy of 5–7 %. When straggling data for hydrogen and helium penetrating the same monatomic gas are compared, significant deviations from the Z_1^2 scaling contained in the Bohr expression for energy straggling Ω_B^2 are observed. These deviations are explained by an atomic correlation term stemming from the bunching of electrons into atoms and by an additional straggling term Ω_C^2 resulting from charge-state fluctuations. It is shown that the importance of charge-exchange straggling has been substantially overestimated in the past. For hydrogen ions penetrating heavy monatomic gases, the straggling increases with increasing energy and approaches the high-energy Bohr limit, in agreement with theory. The qualitative agreement between these hydrogen results and the electron-gas calculations by Bonderup and Hvelplund and by Chu is, however, markedly improved by inclusion of the atomic correlation term. For hydrogen and helium targets, an excess over the Bohr value, caused by finite values of the electron velocities compared to that for the projectile, is observed at velocities, where the electronic stopping power has its maximum. For molecular gases, a further increase in straggling is seen, caused by bunching of atoms into molecules, which leads to a further increase in the fluctuations of the number of collisions with electrons.

Institute of Physics, University of Aarhus
DK-8000 Aarhus C, Denmark.

Printed in Denmark by Bianco Lunos Bogtrykkeri A/S. ISSN 0023-3323. ISBN 87-7304-113-0.

Contents

§ 1. Introduction

When an initially monoenergetic ion beam penetrates matter, the average energy loss is accompanied by a spreading of the energy of the ion beam due to the statistical nature of the collision processes. A measure of this energy broadening is given by the mean-square deviation Ω^2 of the resulting energy-loss distribution, also known as the energy straggling.

While the average energy loss per path length, the so-called stopping power, of energetic hydrogen and helium ions has been extensively studied and can be predicted to within 3–10 % for all elements from recent tabulations (Andersen and Ziegler (1977) and Ziegler (1978)), the straggling in energy loss has received much less attention, probably because straggling measurements involve more experimental complications than do stopping-power measurements, and most of the published experimental straggling results are thus rather uncertain. However, as Rutherford-backscattering and nuclear-reaction analysis have become important microanalytical techniques for discerning atomic mass, resolving depth, and perceiving crystalline structure of the near-surface region of materials, precise data on energy straggling are desirable since electronic energy-loss straggling is indeed one of the main features limiting the depth resolution of both these ion-beam-analysis teckniques.

The fact that the majority of experimental straggling results have been obtained using solid targets has obscured our understanding and description of the straggling processes since specific solid-state effects stemming from target inhomogeneities such as nonuniform film thickness, porosity, surface contamination, and crystal structure can obscure the measured straggling in an uncontrolable way. Measurements with gaseous targets provide a much better basis for quantitative comparison between theory and experiment, and we have therefore performed an accurate, systematic investigation of the straggling in energy loss for hydrogen and helium ions on a variety of atomic and molecular gases (H_2, He, N_2, O_2, CO_2, Ne, Ar, Kr, and Xe) at ion energies of $40\ \text{keV} \lesssim E_H \lesssim 1\ \text{MeV}$ and $100\ \text{keV} \lesssim E_{He} \lesssim 2.4\ \text{MeV}$.

The present paper belongs to a series of three, which describes the results of an experimental study of the penetration of swift hydrogen and helium ions through gases [Besenbacher (1977)]. The stopping-power results and a detailed discussion of the experimental setup was presented in the first paper [Besenbacher et al. (1979)], hereinafter referred to as I. In the second paper [Besenbacher et al. (1980)], referred to as II, a comprehensive discussion of the theoretical descrip-

tion of straggling in energy loss of energetic hydrogen and helium ions was presented. The present paper deals mainly with a presentation of the experimental straggling results, some of which have been published in a recent letter [Besenbacher et al. (1977)] and in II.

Following a review of the theory of electronic energy straggling for light, swift ions in § 2, we shall give a brief description of the experimental procedure and data treatment in § 3 together with a discussion of how the measured straggling results are influenced by the small contribution from nuclear collisions. Finally, in § 4, the experimental results are presented and discussed in connection with a comparison with theory.

§ 2. Theory

A general description of the statistical nature of the energy-loss processes in targets with randomly distributed atoms has been given by Bohr (1948). For a monoenergetic beam suffering an energy loss, which is small compared to the initial energy (the thin-absorber approximation), Bohr divided up the collisions of the projectile into various types of processes i, each one corresponding to a small interval of energy transfer $(T_i, T_i + dT_i)$. If n_i denotes the fluctuating number of processes of type i, the average energy loss and the average square fluctuation in energy loss is given by

$$\overline{\Delta E} = \sum_i \overline{n_i} T_i = N \Delta R \int d\sigma(T) = N \Delta R S \tag{1}$$

and

$$\Omega^2 = \overline{(\Delta E - \overline{\Delta E})^2} = \sum_i \overline{(n_i - \overline{n_i})^2} T_i^2 = \sum \overline{n_i} T_i^2 = N \Delta R \int d\sigma(T) T^2 \tag{2}$$

Here, $N\Delta R$ is the target density, $d\sigma$ is the cross section for an energy transfer T, and S is the stopping cross section. The two important assumptions underlying Eqs. (1) and (2) are that processes of different type are statistically independent and that the number of processes of a given type follows Poisson statistics.

As argued by Bohr (1948) and Vavilov (1957), the energy-loss distribution is expected to be a Gaussian provided all the individual contributions to the energy loss are small compared to Ω, i.e., $\Omega \gtrsim 3T_{max}$, where T_{max} is the maximum energy transfer in a single collision with a free electron. This inequality, together with the requirement that $\Delta E \ll E$, leads to the following condition on the target density,

$$E/S \gg N \Delta R \, [\text{atoms/cm}^2] \gtrsim 2 \times 10^{20} \frac{1}{Z_2} \left(\frac{E[\text{MeV}]}{Z_1 M_1 [\text{amu}]} \right)^2, \tag{3}$$

where Z_1, M_1, and E denote the atomic number, mass, and energy of the projectile and Z_2 the atomic number of the target atoms. This requirement defines a broad, experimentally accessible and interesting region, in which comparison between experimental data and theoretical results is most easily performed since the resulting Gaussian energy-loss distribution is characterized by $\overline{\Delta E}$ and Ω only. The general case, for which the inequalities in Eq. (3) are not necessarily fulfilled, has been treated by Bohr (1948) and, in particular, by Williams (1929), Landau (1944), Vavilov (1957), and Tschalär (1968). In the limit of very thin ($\Omega \ll T_{max}$) and very thick ($\Delta E \sim E$) absorbers, highly asymmetric energy-loss distributions are obtained.

For the light, swift ions considered in this experiment, the slowing-down is mainly caused by collisions with electrons. Assuming as a first approximation that all the target electrons contribute to the straggling as free electrons initially at rest, we may insert in Eq. (2) as the differential cross section the Thomson formula for the scattering of a projectile with velocity v by a free electron,

$$d\sigma = -\frac{2\pi Z_1^2 e^4}{mv^2}\,\frac{dT}{T^2}\,, \tag{4}$$

where $-e$ and m denote the charge and mass of the electron. As opposed to the calculation of the average energy loss, the Rutherford cross section may provide a reasonable approximation to be used in the calculation of energy straggling since this quantity is dominated by the more violent collisions, for which atomic binding and screening are less important. By inserting Eq. (4) into Eq. (2), we obtain Bohr's remarkably simple nonrelativistic high-energy limit,

$$\Omega^2 = \Omega_B^2 = 4\pi Z_1^2 e^4 Z_2 N \Delta R\,. \tag{5}$$

So far, the orbital velocities v_e of the electrons have been completely neglected as compared to the projectile velocity v. For small but finite values of v_e/v, a correction term to the simple Bohr formula appears, and in the quantal-perturbation limit $v \gg 2Z_1 v_0$, where $v_0 = e^2/\hbar$, the following formula is obtained [Fano (1963)],

$$\frac{\Omega_F^2}{\Omega_B^2} = 1 + \frac{\frac{1}{Z_2}\,S(1)}{mv^2}\log\frac{2mv^2}{I_1}\,. \tag{6}$$

Here, the average excitation energy I_1 is given in terms of the atomic dipole oscillator strengths f_{0i} and the corresponding transition frequencies ω_{0i} by

$$\log I_1 = \frac{\sum_i f_{0i}\hbar\omega_{0i}\log\hbar\omega_{0i}}{\sum_i f_{0i}\log\hbar\omega_{0i}}\;;\;\sum_i f_{0i} = Z_2\,, \tag{7}$$

while the parameter S(1) defined as the zero moment over the dipole oscillator-strength distribution according to Fano (1963) can be written as

$$S(1) = \sum_i \hbar\omega_{0i} f_{0i} = \frac{2m}{3} < \left| \sum_i v_i \right|^2 >_0 , \tag{8}$$

where v_i is the velocity of the i'th atomic electron and $< >_0$ denotes the ground-state expectation value. The validity of Eq. (8) is discussed in some detail in Sec. 4.3.

As the velocity of the projectile decreases, the velocity of the inner electrons may even exceed the projectile velocity, especially for heavy substances. According to Bohr (1948), an approximate way of accounting for the straggling in this situation is to neglect the contribution to the straggling from the inner electrons and replace the total electron density NZ_2 in Eq. (5) by the density of electrons with velocities lower than v. For this density, Bohr inserted the value $N(v_e < v) \sim NZ_2^{1/3}(2v/v_0)$, and at lov velocities, this implies a significant reduction in the straggling compared to the Bohr value.

Bohr's treatment was improved by Lindhard and Scharff (1953). They treated the target as a collection of free electron gases, and the straggling pertaining to an atom was obtained as an average over the electron cloud of the straggling $\Omega^2(\varrho, v)$ for a gas of constant density ϱ (see Eq. (7) in II). In order to calculate $\Omega^2(\varrho, v)$, the electron cloud of the target atom is divided into an outer and an inner region, where the outer electrons are roughly those corresponding to a local Fermi velocity lower than v. Assuming that the contributions from the outer and inner electrons are given by the asymptotic expressions for an electron gas and using the Bohr model for the atomic density $\varrho(r)$, Lindhard and Scharff (1953) arrived at the following formula,

$$\frac{\Omega^2_{LS}}{\Omega^2_B} = \begin{cases} \dfrac{L(x)}{2} & \text{for } x \lesssim 3 \\ 1 & \text{for } x \gtrsim 3 \end{cases} . \tag{9}$$

Here, x is a reduced energy variable, $x = (v/v_0)^2/Z_2$, and L(x) is defined in terms of the electronic stopping cross section through the relation

$$S_e = \frac{1}{N}\left(-\frac{dE}{dR}\right) = \frac{4\pi Z_1^2 e^4}{mv^2} Z_2 L(x) . \tag{10}$$

Bonderup and Hvelplund (1971) have refined the Lindhard-Scharff model by using a more accurate expression for the straggling contributions from the various parts of the electron cloud and the more realistic Lenz-Jensen model for the atomic-electron density. Similar calculations with Hartree-Fock-Slater elec-

tron densities have been performed by Chu (1976). These calculations were based on the following expression for $\Omega^2(\varrho,v)$, (Bonderup and Hvelplund (1971)).

$$\frac{\Omega^2_{BH}(\varrho,v)}{\Omega^2_B} = \begin{cases} 1+\left[\frac{1}{5}\left(\frac{v_F}{v}\right)^2+\frac{\hbar\omega_0}{2mv^2}\right]\log\left(\frac{v}{v_F}\right)^2; & v \gtrsim v_F \quad (11a) \\ (1+13\chi^2)^{-1/2}\left(\frac{v}{v_F}\right)^2; & v \lesssim v_F\,, \quad (11b) \end{cases}$$

where $v_F(\varrho)$ is the local Thomas-Fermi velocity, $\omega_0(\varrho)$ is the local plasma frequency, and $\chi^2 = v_0/\pi v_F$ is a dimensionsless quantity proportional to the third root of the density. The term with the plasma frequency stems from resonance collisions due to collective excitations, but the main contribution in the limit $v \gtrsim v_F$ comes from single-particle collisions.

However, as pointed out by Bonderup and Hvelplund (1971) and discussed in greater detail in II, it is important to realize that, within the Lindhard-Scharff (LS) model, the projectile-electron excitations are assumed to lead to the same basic, statistically independent excitations in the atom as in the electron gases by means of which the electron cloud is described. In a real atomic gas target, the electrons are bunched into atoms, leaving part of the space empty. This spatial correlation of the atomic electrons leads to stronger fluctuations in the number of collisions with electrons and thus to an increase in energy straggling. A similar type of correlation results when the target is a dilute gas of diatomic molecules. In this case, the electrons are not only bunched into atoms, but the atoms are also bunched together into molecules, leading to a further increase of the fluctuation in the number of collisions with electrons. These molecular correlation effects have been discussed extensively by Sigmund (1976, 1978) from a somewhat different point of view. Another type of correlation effect may stem from charge-state fluctuations in a gas target, when the charge of the ion fluctuates in such a manner that a given charge state persists during several ion-atom collisions. Since the energy loss depends on the charge state, the losses in successive collisions with atoms become correlated, and an additional straggling contribution Ω^2_B results. Spatial and charge-state correlations were discussed in detail in II, and only the main results will be stated here.

As shown in II, the straggling for a light, swift ion colliding with an atom, which contains many electrons, can, if charge-state fluctuations are neglected, be written as

$$\Omega^2 = \Omega^2_{LS} + \Omega^2_A \quad (12)$$

with the atomic correlation term Ω^2_A given by

$$\Omega^2_A = N\Delta R \int d^2\boldsymbol{p}\,[\varepsilon(\boldsymbol{p})]^2\,. \quad (13)$$

Here, $\varepsilon(\boldsymbol{p})$ is the average energy loss to an atom at fixed impact parameter with respect to the nucleus. In II, it was found convenient to introduce an atomic area,

$$\pi r_A^2 = \frac{[\int d^2\boldsymbol{p}\varepsilon(\boldsymbol{p})]^2}{\int d^2\boldsymbol{p}[\varepsilon(\boldsymbol{p})]^2}, \tag{14}$$

such that Eq. (14) can be written as

$$\Omega_A^2 = N\Delta R\frac{S^2}{\pi r_A^2}. \tag{15}$$

Equation (12) reduces to the Lindhard-Scharff expression in the high-velocity limit, where the probability for electron excitation is small. In the opposite extreme to the LS limit, i.e., at sufficiently low projectile velocities, the penetration of the atom leads to the excitation of several electrons. For a fixed impact parameter, the fluctuation in energy loss may then be neglected, and the entire straggling derives from the statistical distribution of impact parameters, i.e., is given by Eq. (13).

For heavy ions at low velocities, $v < v_0 Z_1^{2/3}$ (v_0 is the Bohr velocity), Firsov (1959) has calculated $\varepsilon(\boldsymbol{p})$ within a Thomas-Fermi treatment. Inserting the Firsov result $\varepsilon_F(\boldsymbol{p})$ in Eq. (13), we get the entire straggling for heavy ions in this low-velocity limit (Hvelplund (1971) and II).

$$\frac{\Omega_{HF}^2}{N\Delta R} = \int_0^\infty \varepsilon_F^2(p)2\pi p dp = (Z_1+Z_2)^{8/3}\left(\frac{v}{v_0}\right)^2 8\times 10^{-15}\,eV^2cm^2/atom. \tag{16}$$

For hydrogen and helium ions, on the other hand, a detailed knowledge of $\varepsilon(\boldsymbol{p})$ is still lacking, and this complicates a calculation of the atomic area πr_A^2, and thereby of the atomic correlation term Ω_A^2. However, as discussed in some detail in II, simple estimates based on the Lindhard-Scharff model [Lindhard and Scharff (1953), Lindhard and Winther (1964), and Bonderup (1967)], for energy loss show (i) that πr_A^2 depends only weakly on Z_2, (ii) that for energies around the stopping-power maximum where Ω_A^2 has its maximum value, πr_A^2 is $\sim 8\text{-}10\pi a_0^2$ (a_0 is the Bohr radius) and (iii) that the energy dependence of πr_A^2 is probably rather weak. In II it was therefore tentatively suggested that the simple formula (15) with an atomic area $\pi r_A^2 \simeq 10\pi a_0^2$ may account for the increase in straggling for an atomic-gas target due to the bunching of the electrons. This suggestion is supported at least for protons and α particles by comparison with the comprehensive set of straggling results presented here, a fact that will be discussed in detail in § 4.1.

If, instead, the projectile penetrates a target of homonuclear diatomic mole-

cules with internuclear distance d, the total straggling is obtained by adding to Eq. (12) a further correlation term Ω_M^2, which results from the bunching of the atoms into molecules. For the simple case, where the molecular axis is aligned with respect to the beam axis, the molecular term Ω_M^2 equals Ω_A^2. A misalignment reduces the molecular term, and a simple geometrical argument presented in II as well as a more refined calculation [Sigmund (1976)] yields the following molecular correlation term,

$$\Omega_M^2 = \begin{cases} N\Delta R \dfrac{S^2}{2\pi d^2}, & d \gg r_A \qquad (17a) \\ \Omega_A^2 = N\Delta R \dfrac{S^2}{\pi r_A^2}, & d < r_A \qquad (17b) \end{cases}$$

Concerning the straggling contribution stemming from charge-state fluctuations, the discussion will be restricted to target thicknesses, for which several charge-changing collisions occur, and to cases where only two charge states q_1 and q_2 are important. This is the situation for helium ions at the energies and target thicknesses used in the present work. If S_1 and S_2 denote the stopping cross section for the projectile in the two charge states and α is the fractional time spent in charge state 1, the average-square fluctuation in ΔE due to fluctuations in α is given by

$$\Omega_C^2 = (N\Delta R)^2 (S_1 - S_2)^2 (\overline{\alpha^2} - \bar{\alpha}^2) . \qquad (18)$$

The average-square fluctuations in α is determined by the capture and loss cross sections σ_{12} and σ_{21}, and a calculation presented in II yields

$$\Omega_C^2 = N\Delta R \, (S_1 - S_2)^2 \frac{2\sigma_{12}\sigma_{21}}{(\sigma_{12} + \sigma_{21})^3} . \qquad (19)$$

This result is similar to that stated by Vollmer (1974) and by Efken et al. (1975).

§ 3. Experimental procedure and data treatment

In the present work, an extensive investigation of energy loss and straggling in energy loss for hydrogen ions of 40-keV to 1.5-MeV energy and helium ions of 100-keV to 2.4-MeV energy penetrating thin layers of various gases (H_2, He, N_2, CO_2, O_2, Ne, Ar, Kr, Xe) has been carried out.

Since details of the experimental procedure and data treatment were presented in I, only a brief description will be given here.

A magnetically analyzed hydrogen or helium beam passes through a differentially pumped, 504-mm long gas cell via 0.2-mm diameter apertures. For energies below 300 keV, measurements were performed at a 400-kV Van de Graaf accelerator and a 100-kV electromagnetic isotope separator. The energy-degraded beam was energy-analyzed by means of an electrostatic analyzer and detected

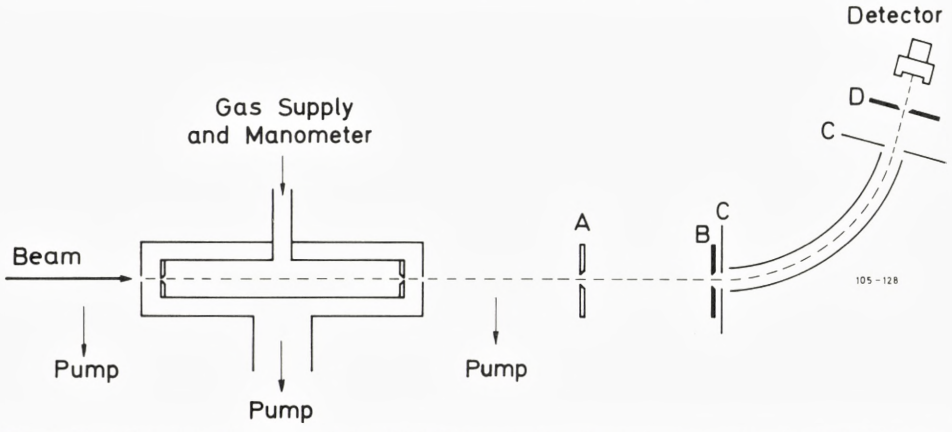

Fig. 1: Experimental setup used at the 400-kV Van de Graaff accelerator and at the 100-kV isotope separator.

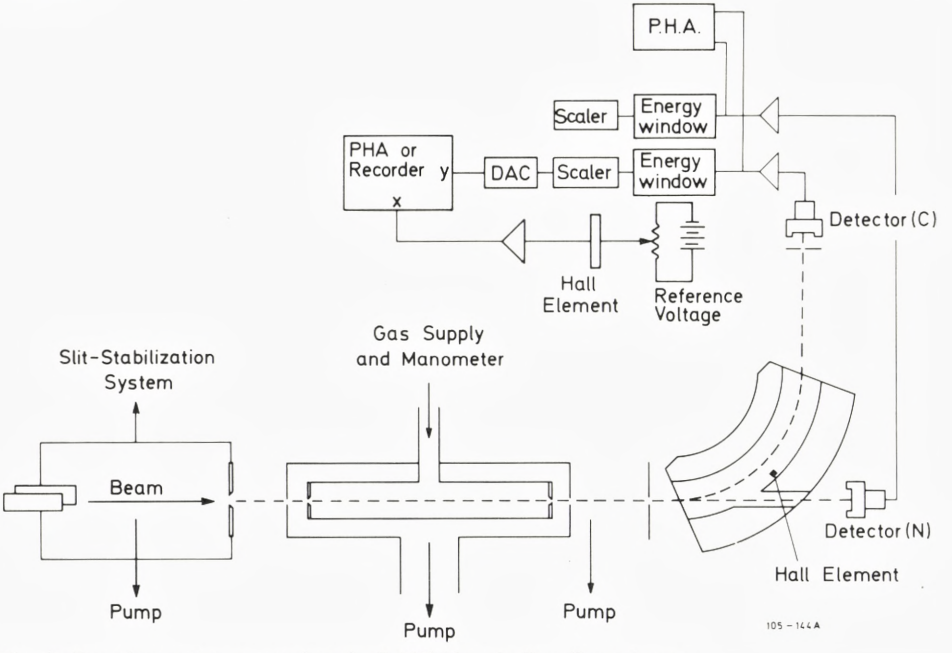

Fig. 2: Experimental setup used at the 2-MV Van de Graaff accelerator.

by a standard Si surface-barrier detector, as shown in Fig. 1. The energy-loss distributions were measured by sweeping the beam across the exit aperture D by means of the electrostatic analyzer. In this way, the beam intensity is averaged in time, and no beam normalization is needed. For energies above 200 keV, measurements were performed at a 2-MV Van de Graaff accelerator, and the beam transmitted through the gas cell was momentum-analyzed, using a double-focussing sector magnet, and detected by a solid-state detector (Fig. 2). Detector N counted neutrals and was used for normalization. Thus fluctuations in the beam current did not influence the measurements. The use of energy-dispersive detectors allowed elimination of beam contamination and slit-edge-scattered particles. The pressure in the gas cell was measured with a membrane manometer, and the pressure was kept stable within less than 1 % via a motor-driven, servo-controlled needle valve. The purity of all gases used was better than 99.5 %.

In all cases except for hydrogen ions penetrating H_2 at energies above 200 keV, the gas-cell pressure ($0.1 \lesssim P_G \lesssim 2$ torr) was chosen to satisfy the inequalities (3), which give Gaussian energy-loss distributions. This was confirmed experimentally by plotting the distribution on graph paper with a cumulative Gaussian scale, as shown by the example given in Fig. 3.

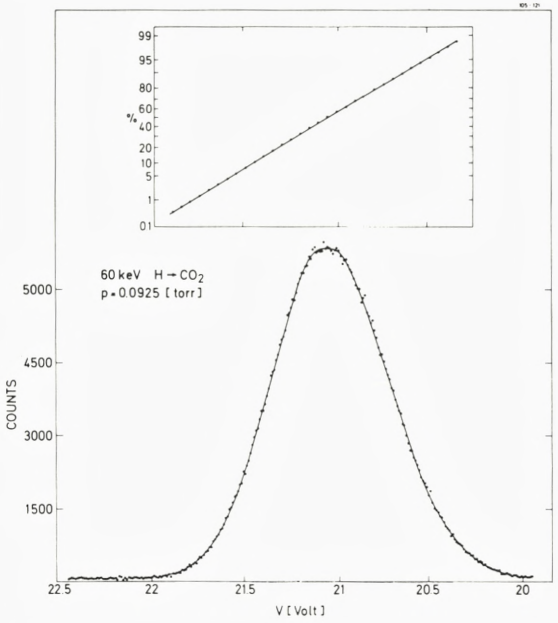

Fig. 3: Energy distribution of an incident 60-keV H^+ beam after it emerges from a 1.51×10^{17} molecules/cm^2 CO_2 layer. The main part of the distribution is plotted on probability paper, from which it is concluded that the energy-loss distribution is Gaussian.

From the measured energy-loss or momentum distribution, the average energy loss and the standard deviation are easily obtained as

$$\overline{\Delta E} = E_i - \frac{E_1 + E_2}{2} \tag{20}$$

and

$$\Omega_E = \frac{E_1 - E_2}{2\sqrt{2\log 2}} \tag{21}$$

where E_i is the incident energy and E_1 and E_2 are the energies corresponding to the half-maximum positions for either the momentum or the energy-loss distribution. The energy spectra obtained with no target gas were also approximately Gaussian with a mean-square deviation Ω_i, corresponding to an energy resolution (FWHM/E_i) of 0.74 % and 0.10 % for the electrostatic and the magnetic analyzers, respectively. Consequently, the straggling can be obtained from the formula

$$\Omega^2 = \Omega_E^2 - \Omega_i^2 \,. \tag{22}$$

In all the cases reported here, Ω_i is small compared to Ω_E. The target density $N\Delta R$ in molecules/cm^2 is calculated from Eqs. (15) and (16) in I, and the straggling parameter $\Omega^2/N\Delta R$ is assigned to the mean energy $E_{av} = E_i - \Delta E/2$.

For asymmetric energy distributions, which were found only for hydrogen penetrating H_2 at energies $E \gtrsim 200$ keV, the moments $M_1 = \overline{\Delta E}$ and $M_2 = \Omega^2$ were found by numerical integration of the energy-loss distribution $W(\Delta E)$ according to

$$M_1 = \frac{\int_0^\infty \Delta E\, W(\Delta E)\, d(\Delta E)}{\int_0^\infty W(\Delta E)\, d(\Delta E)} \tag{23}$$

$$M_2 = \frac{\int_0^\infty (\Delta E - \overline{\Delta E})^2\, W(\Delta E)\, d(\Delta E)}{\int_0^\infty W(\Delta E)\, d(\Delta E)} \tag{24}$$

To verify that the straggling Ω^2 is proportional to the target density $N\Delta R$, Ω^2 was plotted versus $N\Delta R$ for different energies and gases, and a typical example is shown in Fig. 4.

In the present energy region, it is not possible to correct in a simple way the measured straggling data for contributions from nuclear collisions as is the case for stopping-cross-section data. The reason is that compared to average energy

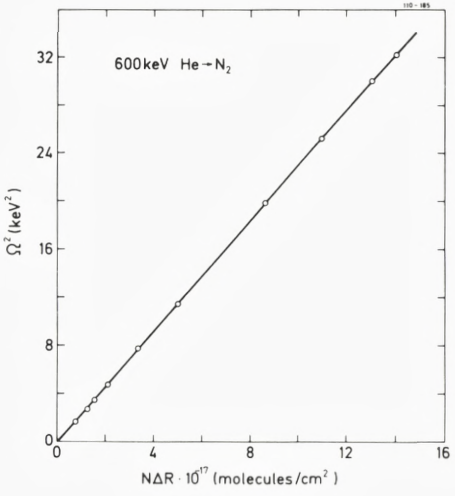

Fig. 4: The energy straggling Ω^2 versus target density for He in N_2.

loss, straggling depends more strongly on close collisions, and hence the separation of the elastic and inelastic collisions becomes more ambiguous. In order to estimate the contribution from nuclear collisions to the measured straggling, we shall consider the following example, which represent one of the cases with the largest contribution from nuclear collisions,

113.4 keV He → He	$N\Delta R = 1.24 \cdot 10^{18}$ atoms/cm^2
$\Omega_e = 0.792$ keV	$\Omega_n = 1.137$ keV
$T_{max,e} = 0.062$ keV	$T_{max,n} = 113.4$ keV

Here, indices e and n refer to electronic and nuclear collisions, respectively, and Ω_n is calculated from Bohr's nuclear-straggling formula (Bohr (1948)), which is analogous to formula (5). The spectrum originating from the electronic collisions will be a Gaussian distribution, while the nuclear collisions give rise to a strongly asymmetric distribution with a low-energy tail. However, particles which have experienced the most violent nuclear collisions are scattered out of the angularly narrow, forward-directed, analyzed beam, thus reducing the "nuclear tail" considerably. According to Hvelplund (1971), the particles accepted by the analyzer will approximately be those which have suffered collisions with an energy transfer $T \lesssim T_n^*$ where T_n^* is the nuclear-energy transfer, corresponding to a deflection angle φ^* that divides the angular distribution into a Gaussian peak and a tail. In Fig. 5, T_n^* and the corresponding impact parameter p_{min} are shown for the case considered here. If the measured straggling is given by

$$\frac{\Omega^2_{exp}}{N\Delta R} = \int_{p_{min}}^{\infty} (T_n + T_e)^2 2\pi p dp, \qquad (25)$$

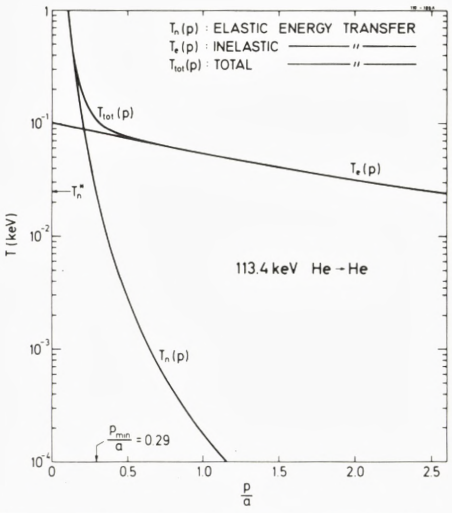

Fig. 5: Energy transfer in a single collision as a function of impact parameter. Inelastic transfer is calculated from Firsov's (1959) $T_e(p)$. The elastic energy transfer is calculated from a power potential $V(r) \propto r^{-2}$ (Lindhard et al. (1968)). T_n^* and p_{min} refer to maximum elastic energy transfer and the corresponding impact parameter for atoms still belonging to the forward-directed beam, cf. text. The TF screening radius is given by $a = 0.8853\, a_0 (Z_1^{2/3} + Z_2^{2/3})^{-1/2}$.

then for the actual case $\Omega_{exp} > T_e(p_{min}) + T_n^*$, and hence the energy distribution for the forward-directed beam should be Gaussian, in agreement with the experimental findings. From Fig. 6 it is found that the contribution from the nuclear collisions (area I_2) to the measured straggling Ω_{exp}^2 is roughly 2 %, whereas the excluded straggling term from electronic collisions with $p < p_{min}$ (area I_1) is approximately 4 %.

It can thus be concluded that the measured straggling can be attributed mainly to electronic collisions, and no corrections for nuclear straggling have been applied.

Based on the systematic and statistical experimental errors quoted in I and an assumed 10 % uncertainty in Ω_i^2 (stemming from the assumption that the primary energy distribution is Gaussian and from the actual value of Ω_1^2), we estimate the total uncertainty in the measured straggling $\Omega^2/N\Delta R$ to be 5–7 %.

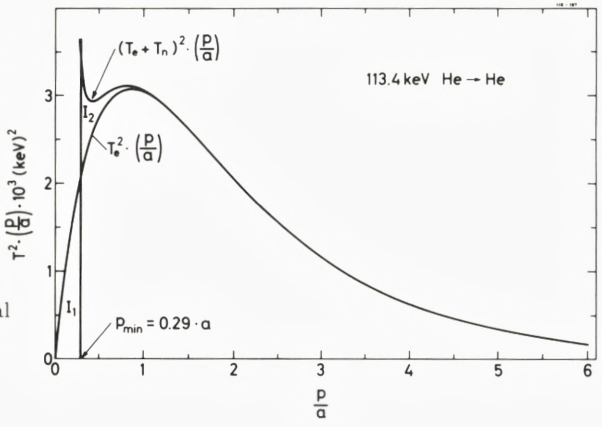

Fig. 6: The energy transfer squared times the reduced impact parameter for the specific case considered in Fig. 5, plotted versus the reduced impact parameter. According to formula (25), the contribution to the straggling from nuclear collisions is given by the area I_2 and the straggling term stemming from small impact parameters, which we exclude in the present experimental setup, is given by the area I_1. Concerning T_e, T_n, and p_{min}, see Fig. 5.

§ 4. Experimental results and comparison with theory

4.1 *Deviations from* Z_1^2 *Scaling for* H *and* He *Ions in Monatomic Gases*

Since the contributions to the Lindhard-Scharff straggling term in Eq. (13) mainly stems from close collisions with electrons, Ω_{LS}^2 is proportional to Z_1^2 even in an energy region where the electronic stopping power may deviate from the Z_1^2 perturbation scaling. The corrections to Ω_{LS}^2, however, show a different dependence on Z_1 since they are proportional to S_e^2 and thus to $\sim Z_1^3 - Z_1^4$. It is therefore possible to obtain a semi-emperical determination of the atomic-correlation term Ω_A^2 due to bunching of electrons into atoms by comparing experimental hydrogen- and helium-straggling results for the same monatomic gas. As argued for in II, such a semiempirical procedure is preferable because of the problems involved in performing a stringent theoretical calculation of Ω_A^2.

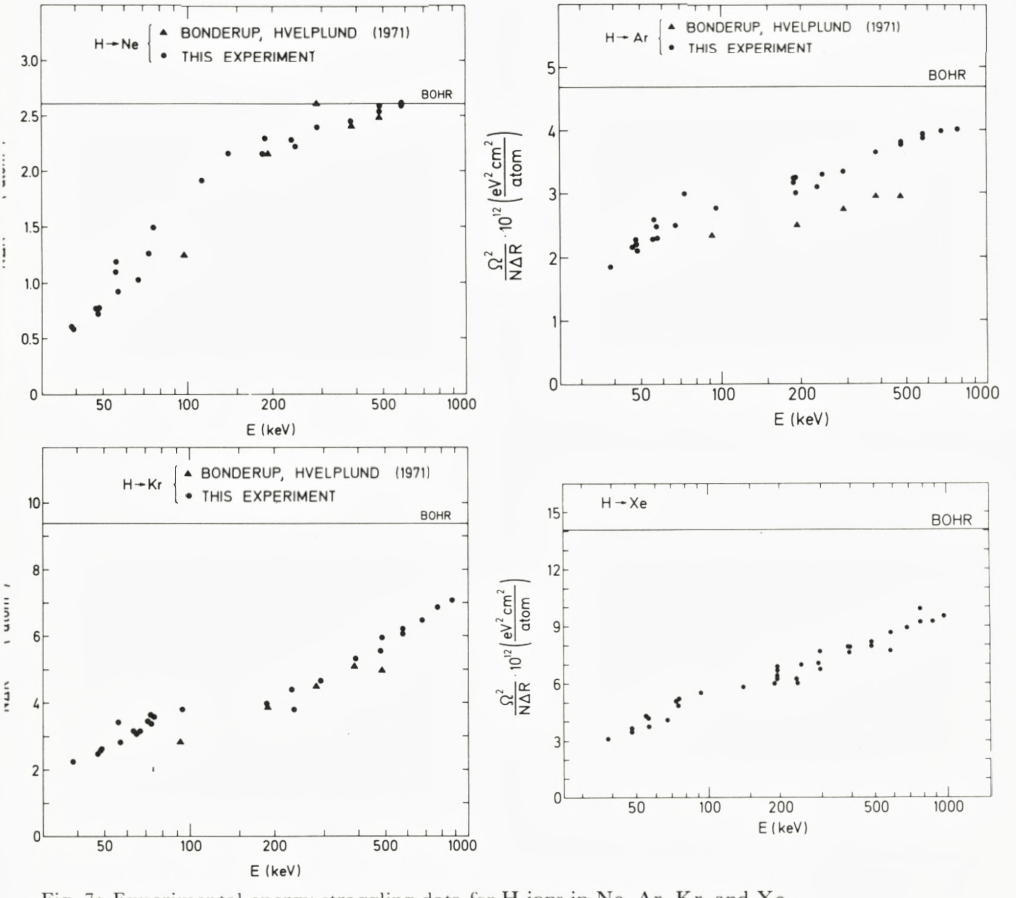

Fig. 7: Experimental energy-straggling data for H ions in Ne, Ar, Kr, and Xe.

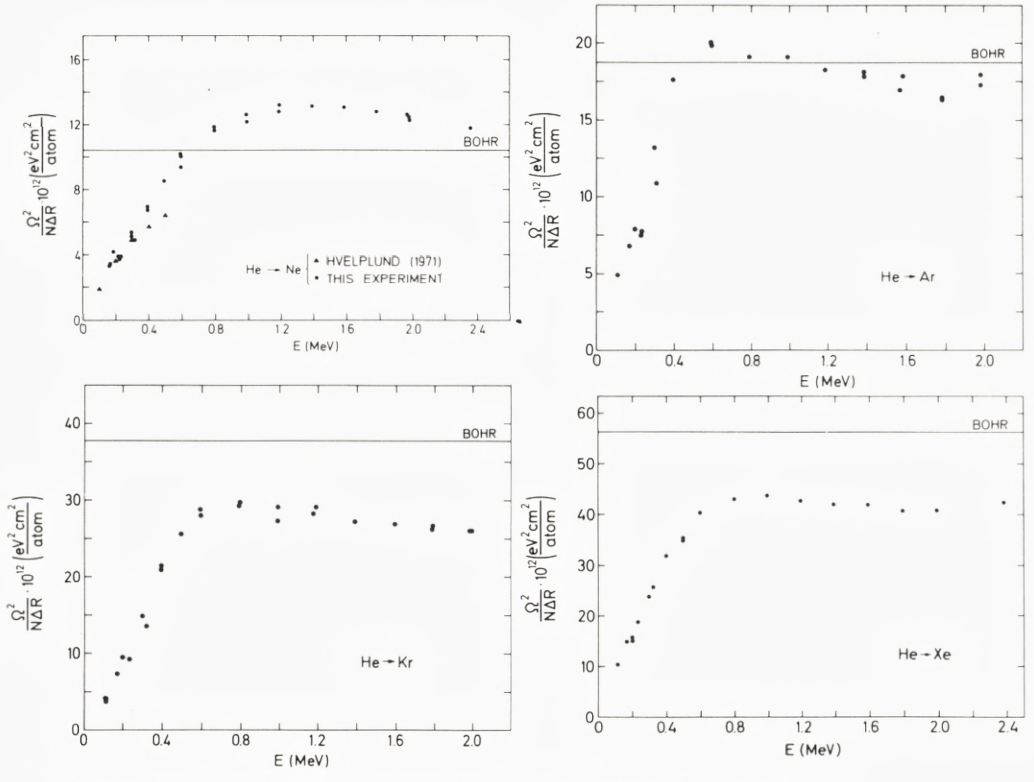

Fig. 8: Experimental energy-straggling data for He ions in Ne, Ar, Kr, and Xe.

The experimental straggling parameters $\Omega^2/N\Delta R$ for hydrogen and helium ions penetrating Ne, Ar, and Xe are plotted in Figs. 7 and 8 as a function of the mean energy E_{av}. While the hydrogen data increase monatomically and approach the Bohr value for increasing energy, as expected from theory, the helium data show a local maximum at $E_{He} \sim 1$ MeV. In Fig. 9, the hydrogen and helium results Ω^2/Ω_B^2 are plotted versus energy per nucleon for Ne, Ar, Kr, and Xe, while similar results for a helium target are shown in Fig. 15. A significant deviation of the Ω^2 values from the Z_1^2 scaling contained in the Bohr straggling formula Ω_B^2 (Eq. (5)) is revealed. The difference between the averaged helium and hydrogen results in Figs. 9 and 15, which is plotted as points in Figs. 10 and 16, can, as argued above, be attributed to corrections to the Lindhard-Scharff term, i.e., to straggling terms resulting from the bunching of electrons into atoms and from charge-state fluctuations.

The contribution from charge-state fluctuations for helium ions can be obtained from Eq. (20) and is shown in Figs. 10 and 16 as the lower solid line. For

Fig. 9: Energy straggling for H and He ions in Ne, Ar, Kr, and Xe versus energy per nucleon. The solid lines through the experimental results are drawn only to guide the eye.

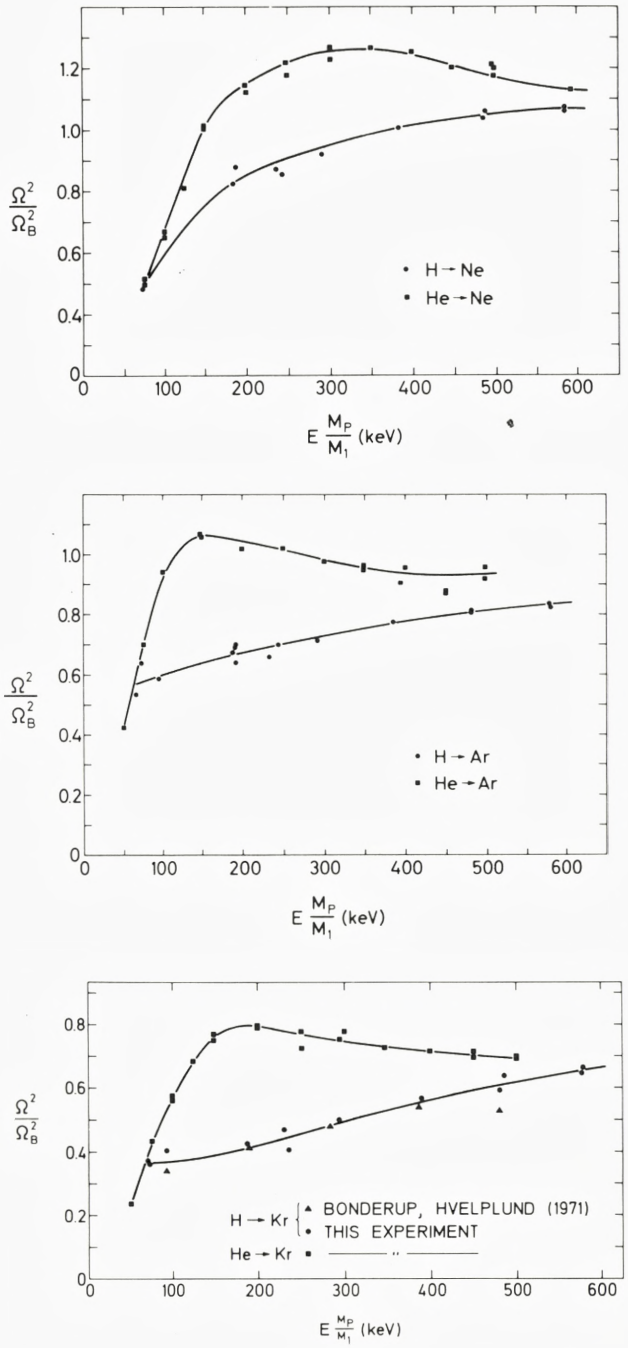

Fig. 9 continued on p. 20.

Fig. 9 (continued from p. 19).

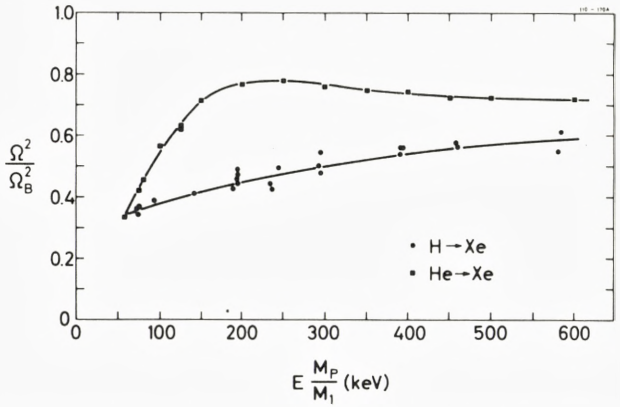

the capture and loss cross sections in Eq. (20), the experimental values for Kr, Ar, and He of Pivovar et al. (1962a, 1962b) and of Hvelplund et al. (1976, 1980) are used while no data are available for Ne and Xe. A simple estimate of the partial stopping cross section $S_e(He^+)$, i.e., the stopping cross section of a helium ion in the fixed charge state He^+ (Cuevas et al. (1964)) can be obtained from our measured helium-stopping cross sections (I) through the equation

$$S(He) = F_{1\infty} S_1(He^+) + F_{2\infty} S_2(He^{++}) , \qquad (26)$$

for $E_{He} \gtrsim 400$ keV, for which the neutral component is negligible. Here, the equilibrium charge-state fractions are given by $F_{1\infty} = \sigma_{21}(\sigma_{12} + \sigma_{21})^{-1}$ and $F_{2\infty} = \sigma_{12}(\sigma_{12} + \sigma_{21})^{-1}$, while the partial α-stopping cross section $S_2(He^{++})$ can be set equal to four times the measured proton-stopping cross section S_p (I). The uncertainty in the derived straggling contribution Ω_C^2/Ω_B^2 is ~ 15–25 %, stemming from uncertainties in the applied experimental quantities. For the heavy monatomic gases, it is seen in Fig. 10 that Ω_C^2 is negligible for $E\frac{M_p}{M_1} \gtrsim 300$ keV and that Ω_C^2/Ω_B^2 cannot alone account for the experimental helium-hydrogen difference.

In previous investigations of the influence of charge-exchange straggling [Besenbacher et al. (1977) Bednyakov et al. (1977), Efken et al. (1975), Sofield et al. (1978), Crowern et al. (1979), Schmidt-Böcking and Hornung (1978), Vollmer (1974)], it has been assumed that the partial stopping cross section of an ion in a fixed charge state q can be written as $S_q = q^2 S_p$, which for the factor in Eq. (19) yields $(S_1 - S_2)^2 = (q_1^2 - q_2^2)^2 S_p^2$. For helium ions, this means that $S_1(He^+) = S_p$, which is appropriate for distant collisions only, and consequently, $S_1(He^+)$ is underestimated. The assumption thus leads to values of Ω_C^2/Ω_B^2, presented by the upper full-drawn curves in Figs. 10 and 16, which overestimate the influence of charge-state fluctuations considerably.

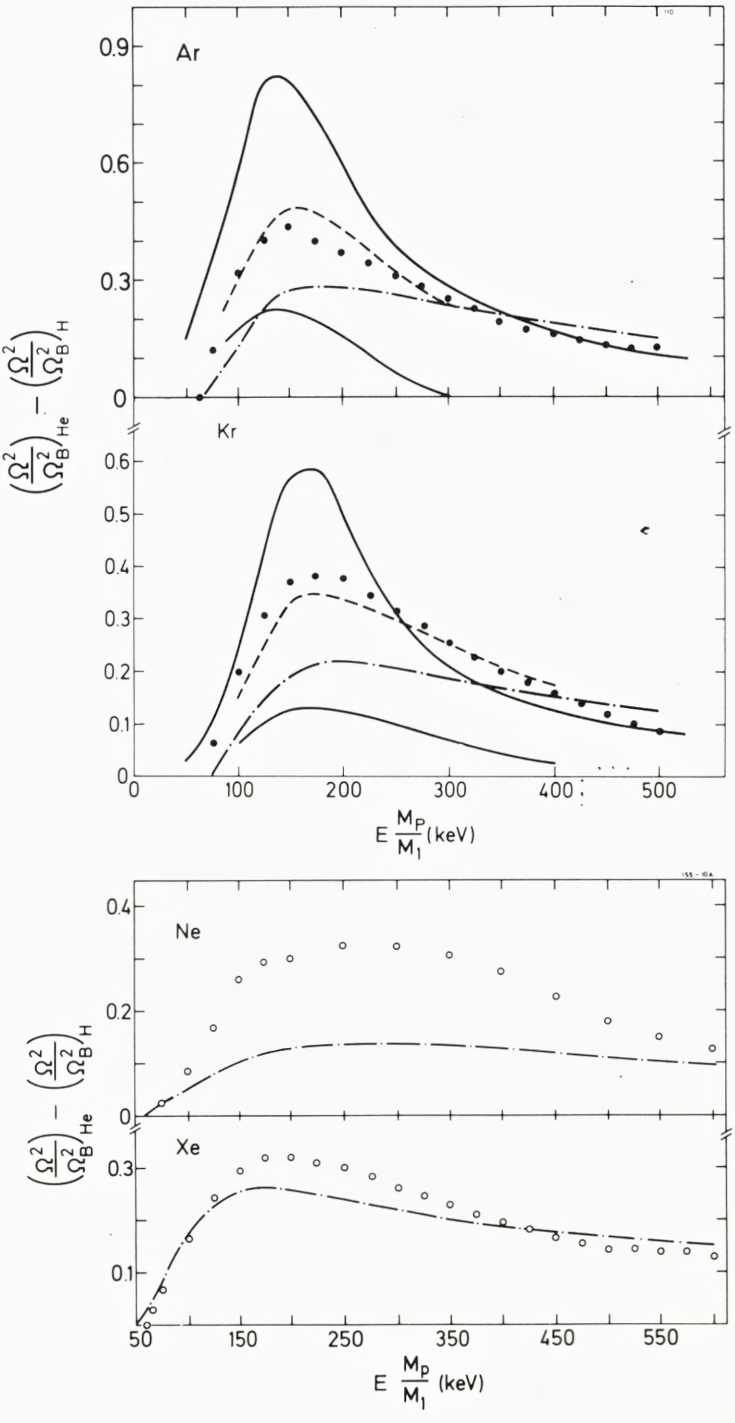

Fig. 10: The deviation from the Z_1^2 scaling of energy straggling for H and He ions in Ar, Kr, Ne, and Xe versus energy per nucleon. The points display the difference between the experimental He and H results from Fig. 9. The contribution from charge-state fluctuations Ω_C^2 (Eqs. (19) and (26) for He ions, measured in units of Ω_B^2 (He), is given by the lower, solid curve, whereas the upper solid curve shows the incorrect value of Ω_C^2 calculated previously under the assumption that the stopping cross section for He^+ is equal to that for protons. The difference between the atomic-correlation terms in units of Ω_B^2 for He and H ions is represented by the dot-and-dash curve for an atomic area of $10\pi a_0^2$. When the contribution from charge-state fluctuations is added, the dashed curve results.

The difference between the atomic correlation terms Ω_A^2/Ω_B^2 for helium and hydrogen ions is shown as the dot-and-dash curve in Figs. 10 and 16. For Ω_A^2 we have used Eq. (15) with the experimental-stopping cross section (I) and an atomic area πr_A^2 of $10\pi a_0^2$. Adding to this curve the contribution from charge-state fluctuations, we obtain the dashed curve, which is seen to be in overall good agreement with the experimental data. This fact lends strong support to the theoretically predicted expression for the atomic correlation term (Eq. (15) with an atomic area $\pi r_A^2 \simeq 10\pi a_0^2$, approximately independent of energy and Z_2.

For a xenon target, the helium-hydrogen difference is nearly completely described by Ω_A^2; for the medium elements such as Kr, Ar, and Ne, the relative importance of Ω_C^2 increases with decreasing atomic number, and for helium, the difference can on the whole be accounted for by Ω_C^2. The experimental results thus support the expectation that the relative importance of the atomic bunching term Ω_A^2 decreases with decreasing number of target electrons since from Eqs. (15) and (5), we have that Ω_A^2/Ω_B^2 is roughly proportional to Z_2.

While the helium-hydrogen difference in Fig. 10 approaches zero at high energies, negative values are obtained at low energies (see, e.g., the argon and krypton data in Figs. 9 and 10). This at first somewhat surprising result is explained by the energy dependence of the stopping, cross sections and thereby of the atomic correlation term Ω_A^2, Eq. (15). For energies $E\frac{M_p}{M_1} \sim 50$–100 keV, S_H and consequently Ω_A^2 for hydrogen ions reach their maximum values and are approximately constant while S_{He} and hence Ω_A^2 for helium ions decrease with energy as $E^{1/2}$ and E, respectively, and at 50 keV, $(\Omega_A^2/\Omega_B^2)_H$ is in fact larger than $(\Omega_A^2/\Omega_B^2)_{He}$. This explains the steep slope of the dot-and-dash curves in Fig. 10 at the low energies. In Fig. 11, the straggling data for helium and hydrogen ions in Ar have been corrected for the influence of the atomic-straggling term Ω_A^2 due to the bunching

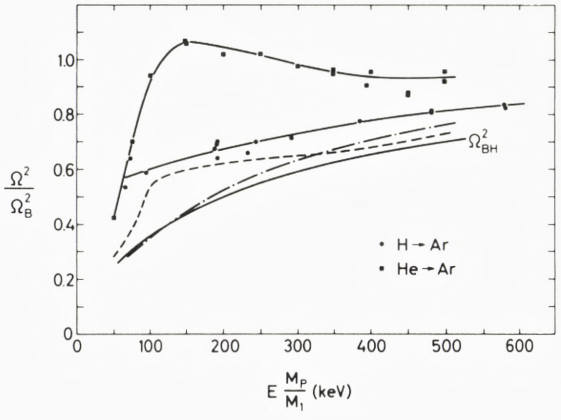

Fig. 11: The experimental-straggling results from Fig. 9 for H and He ions in Ar corrected for the influence of the atomic-straggling term Ω_A^2 given byg Eq. (15) with an atomic area of $10\pi a_0^2$. The corrected He (dashed curve) and H (dot-and dash curve) results are compared with the electron-gas calculations by Bonderup and Hvelplund (1971) (Ω_{BH}^2).

of the electrons into atoms. These corrected helium (dashed curve) and hydrogen (dot-and-dash curve) results agree mutually and with the Bonderup and Hvelplund results (solid curve) both at low and at high energies. The increase of the helium results over the hydrogen results at $E\frac{M_p}{M_1} \sim 50$–100 keV is due to the influence of charge-state fluctuations. Similar curves can be obtained for the other rare gases.

We may complete this section by concluding that the importance of charge-exchange straggling has been overestimated substantially in the past, and that the deviation from the Z_1^2 scaling of Ω^2, resulting in a significant difference between the helium- and hydrogen-straggling results may be accounted for by the atomic bunching term given by Eq. (15) with an empirically determined area of $10\pi a_0^2$ and the charge-exchange straggling expression given by Eqs. (19) and (26).

4.2 *Straggling for Hydrogen Ions in the Monatomic Heavy Gases*

In Fig. 12, the experimental straggling results for hydrogen in Ne, Ar, Kr, and Xe are compared with the electron-gas calculations Ω_{BH}^2 by Bonderup and Hvelplund (1971) shown by the dashed curves. The experimental results are in qualitative agreement with the theoretically predicted reduction in straggling compared to the Bohr value for decreasing velocities, but the quantitative agreement

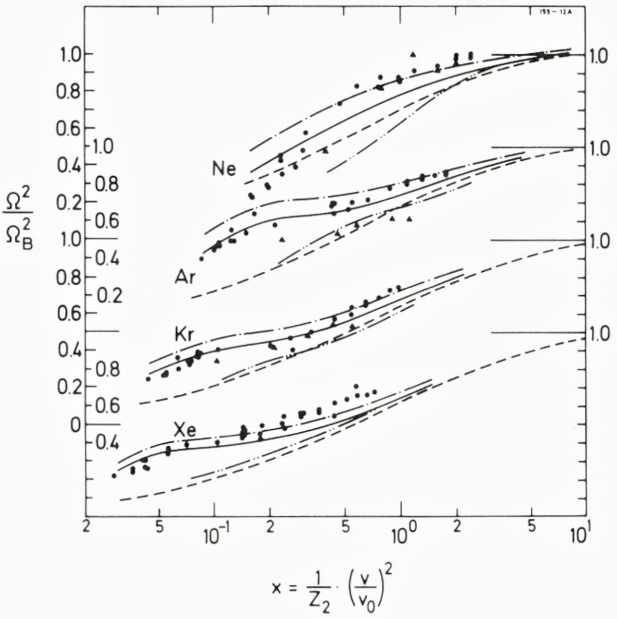

Fig. 12: Energy straggling for protons in Ne, Ar, Kr, and Xe versus the reduced-energy parameter x, normalized to the asymptotic Bohr value (Eq. (5)). The experimental data (•) from Fig. 7 and (▲) from Bonderup and Hvelplund (1971) are compared with the theoretical results. Dashed curves: theoretical values by Bonderup and Hvelplund (1971); solid curves: the sum of the BH results and the atomic correlation term, Eq. (15) for an atomic area of $10\pi a_0^2$; double dot-and-dash curve: theoretical values of Chu (1976); dot-and-dash curve: equivalent to the solid curve except that the BH results are modified, as explained in text.

is rather bad. For the heavier atoms, the discrepancy increases for decreasing x. Adding, however, the atomic correlation term Ω_A^2 given by Eq. (15) with an atomic area of $10\pi a_0^2$ to Ω_{BH}^2, the solid curves in Fig. 11 are obtained, and it is seen that Ω_A^2 on the whole accounts for the discrepancy between Ω_{BH}^2 and the experimental results for Ar, Kr, and Xe, while the agreement in the case of Ne is still relatively poor. However, for the lighter rare gases such as Ne and He, the more realistic Hartree-Fock-Slater electron densities applied by Chu (1976) are superior to the Lenz-Jensen densities underlying the Bonderup-Hvelplund (1971) calculations, and from Fig. 12 it is in fact seen that for Ne, the energy dependence of the measured straggling is in somewhat better agreement with Ω^2_{Chu} (the double dot-and-dash curve). For the heavier elements Ar and Kr, Ω^2_{Chu} and Ω_{BH}^2 are in very good agreement, while Ω^2_{Chu} is systematically 0.05 Bohr units higher than Ω_{BH}^2 for Xe, probably because this element is positioned in a maximum of the Z_2 oscillatory structure in Ω^2 revealed by Chu (1976).

From Fig. 12 the only remaining systematic deviation between theory and experiment appears to be an underestimate of the predicted straggling at higher x values, corresponding to energies above the stopping-power maximum. Since Ω_A^2 in this energy region becomes small, the deviations may be due to uncertainties in Ω_{BH}^2 (Eq. (11)), some of which we shall discuss in the following.

In the straggling calculations by Bonderup and Hvelplund (1971), the target was considered as a collection of free electron gases, and the straggling contribution from an atom was obtained as an average over the electron cloud of the straggling for a gas of constant density. One of the advantages of considering the case of straggling in a free gas of electrons is that one is concerned with a simple scattering phenomenon: An equilibrium situation is established where the projectile is screened by the electron gas or, equivalently, free electrons are scattered in a self-consistent, steady-state screened Coulomb potential. The influence of the screening on the straggling contribution from the outer atomic electrons ($v_e < v$) is of minor importance since for these electrons, the pure Coulomb potential results in the Bohr expression (Eqs. (4) and (5)), which deviates only slightly from the electron-gas expression in Eq. (11a).

However, since the relative contribution from the inner electrons increases with decreasing x (e.g., for $Z_2 = 18$, $\Omega^2_{inner}/\Omega^2_{total}$ takes on the values 0.63, 0.46, and 0.27 at x values of 0.125, 0.41, and 1.52, respectively), the calculated straggling at low x is rather sensitive to the detailed screening prescription used for the contribution from the inner electrons. It might be questionable whether the steady-state screening leading to the explicit dependence of Ω^2_{inner} on the parameter χ^2 in Eq. (11b) is established in a collision with a single atom. One can obtain an overestimate of the straggling contribution from inner electrons by letting the electrons scatter in a pure Coulomb potential around the projectile.

Mathematically, this is equivalent to a replacement of the quantity χ^2 in Eq. (11b) by unity since χ^2 is equal to the ratio $(\lambda\!\!\!^{-}_F/2a)^2$, where $\lambda\!\!\!^{-}_F$ is the wavelength of an electron at the Fermi surface and a is the static screening length in an electron gas ($\lambda\!\!\!^{-}_F = \hbar/mv_F$).

Another type of uncertainty exists in the high-velocity limit of the electron-gas expression given by Eq. (11a). The electrons in an atom are influenced by both the polarization force corresponding to a local plasma frequency ω_0 and an orbital force corresponding to the revolution frequency ω_{rev}. Since $\omega_{rev} \simeq \omega_0$ in the simple Bohr atomic model, Lindhard and Scharff (1953) accounted approximately for the binding of the electrons in the atomic system by multiplying the plasma frequency in the electron-gas calculation by the factor $\sqrt{2}$.

To get an estimate of the uncertainties underlying the electron-gas calculations, those of Bonderup and Hvelplund (1971) have been repeated with the two above modifications of the expressions for the straggling contributions from the outer and inner electrons, and as a result, the solid curves in Fig. 12 are replaced by the dot-and-dash curves. Of the two substitutions, $\omega_0 \rightarrow \sqrt{2}\omega_0$ is the least important, and it only gives rise to a 3 % increase in Ω^2_{BH} at the highest x values. The dot-and-dash curves are in good agreement with the experimental results at the high x values but overestimate the straggling at the low ones, and thus the overall agreement is not improved. The results, however, may indicate that the discrepancies between the experimental results and the theoretical estimates, which are $\sim$10–20 %, are within the accuracy of the electron-gas calculations.

4.3 *Straggling in Light, Monatomic Substances*

The straggling results for hydrogen penetrating helium are shown in Fig. 13, and the data disclose a characteristic "overshoot" above the Bohr value. In Fig. 13 are also plotted the results of the electron-gas calculations by Bonderup and Hvelplund (1971) (dashed curve), and by Chu (1976) (double dot-and-dash curve), together with Fano's straggling formula (6) (solid curve). The parameters I_1 and S(1), which enter this formula, have been calculated by Inokuti et al. (1978) for atomic systems, and in the case of helium, they obtain $I_1 = 80.1$ eV and $S(1) = 104.9$ eV.

The Fano formula is the result of a perturbation calculation, i.e., the probability of an electron excitation is assumed to be small. In principle, all straggling contributions are included in the Fano formula, but in practice, only one-electron excitations are taken into account [Dehmer et al. (1975) and Inokuti et al. (1978)] in calculations of I_1 and S(1). However, as mentioned in Sec. 4.1, the relative importance of the atomic bunching term, which in the Fano treatment can be interpreted as the contribution from multi-electron excitations, decreases with

decreasing Z_2. For helium, the corrections to the Fano curve, with only single-electron excitations included, are therefore expected to be small, but for heavier target elements such as argon, the correction might be important.

For energies $E \gtrsim 300$ keV, the experimental results are in good agreement with Fano's formula, while it fails at low energies, where the assumption $v > v_e$ is no longer fulfilled.

As was the case for neon, the calculations by Chu are superior to those by Bonderup and Hvelplund, and on the whole, the energy dependence of Ω^2_{Chu} agrees with that of the experimental results. The comparison of absolute values is, however, less satisfactory. As shown by the double-dashed curve, this discrepancy cannot be removed through an application of the modified electron-gas expression described above, and the addition of the small atomic correlation term.

In order to understand the difference between Ω^2_{Fano} and Ω^2_{Chu} or Ω^2_{BH}, one has to compare the asymptotic straggling formulas (6) and (11a). The Fano formula is based upon the sum rules for the generalized and the dipole oscillator strengths $F_{0i}(\boldsymbol{q})$ and f_{0i}, and for large and small momentum transfers $\hbar\boldsymbol{q}$, these sum rules are given by

$$\sum_i \hbar\omega_{0i} F_{0i}(\boldsymbol{q}) = \frac{\hbar^2 \boldsymbol{q}^2}{2m} + \frac{4}{3} < K >_0, \quad \text{q large} \tag{27a}$$

$$S(1) = \sum_i \hbar\omega_{0i} f_{0i} = \frac{4}{3}\left[< K >_0 + \frac{m}{2} \sum_i \sum_{j \neq i} < \boldsymbol{v}_i \boldsymbol{v}_j >\right], \quad \text{q small} \tag{27b}$$

where $< K >_0$ is the mean kinetic energy of an electron in the ground state of the target system. Using these sum rules, Fano calculated the contribution from the close and distant collisions, but in the combination of the two contributions to the final formula (6), it was assumed that

$$< K >_0 = \sum_i \hbar\omega_{0i} f_{0i} = S(1) \tag{28}$$

As illustrated by the example of an electron gas, the neglect of the correlation term in Eq. (27b) may be quite serious for the evaluation of the correction to the Bohr formula. In this case, all of the dipole oscillator strength is contained in the plasmon excitation, and the left and right-hand side of Eq. (28) are equal to $2mv_F^2 = (0.12/\chi^2)^{1/2} \cdot \hbar\omega_0$ and $\hbar\omega_0$, respectively. Applying the correct sum rules Eq. ((27)) for an electron gas, we obtain, as expected, the two terms in the square brackets of Eq. (11a). In the high-density limit, $\chi \to 0$, the second term in Eq. (11a) may be neglected, and the constants in front of the logarithms in Eqs. (11a) and (11b) differ by a factor of 2.

In the asymptotic expression (6), shell corrections and other terms of order $< v_e^2 > / v^2$ have been neglected as compared to the logarithm. This may not be a

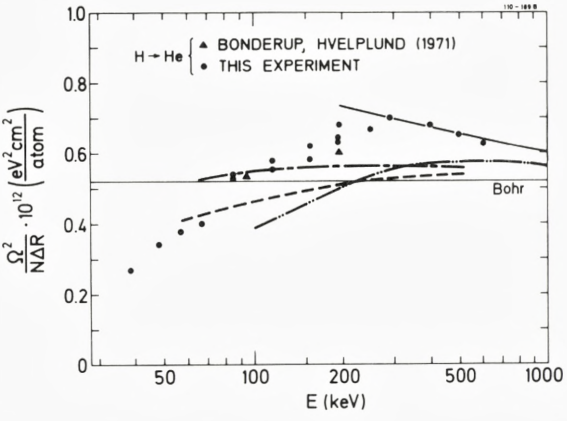

Fig. 13: Experimental energy-straggling data for H ions in He compared with theoretical results. Upper solid curve: the asymptotic Fano straggling formula (6); dashed curve: theoretical values by Bonderup and Hvelplund (1971); double dot-and-dash curve: theoretical values by Chu (1976); — - — curve: Ω^2_{BH}, modified (as explained in text), plus the atomic correlation term, which, in the case of He, is given approximately by Eq. (15) times 0.5 with πr_A^2 equal to $10\pi a_0^2$, cf. II.

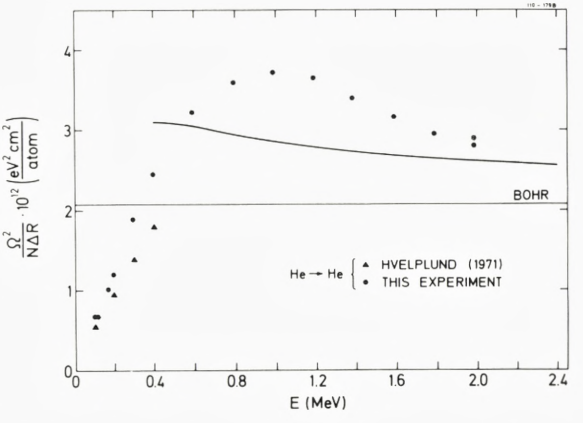

Fig. 14: Experimental energy-straggling data for He ions in He compared with the asymptotic Bohr (1948) (Eq. (5)) and Fano (Eq. (6) straggling formulas (upper solid curve).

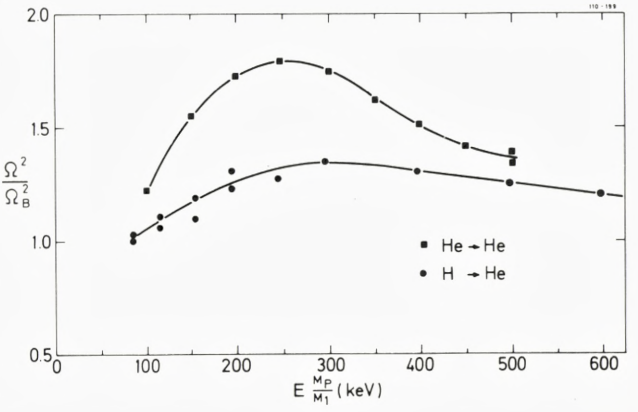

Fig. 15: Energy straggling for H and He ions in He versus energy per nucleon. Solid curves through the experimental data are drawn only to guide the eye.

very good approximation at the relatively low projectile velocities, at which the correction to the Bohr formula becomes significant. Again, the electron gas provides a convenient illustration. The energy I_1 appearing in Eq. (6) is equal to $\hbar\omega_0$, as obtained from the defining equation (7), and at normal atomic electron densities, this energy is quite low as compared to the value $2mv_F^2$ implied by Eq. (11a). To obtain this expression, which was found to be in good agreement with the exact values evaluated numerically by Bonderup and Hvelplund (1971), it was necessary to include terms of order one as compared to terms of order $\log(v/v_F)$ in the expansions. The good agreement between the experimental results and Eq. (6) may therefore be somewhat fortuitous. On the other hand, the statistical description underlying the electron-gas calculations, i.e., Ω^2_{Chu} and Ω^2_{BH}, is probably rather inaccurate for a very light atom such as helium.

In Fig. 14, the experimental straggling results for helium ions transmitted through a helium target are compared to the asymptotic Fano formula (solid curve). Both the energy dependence and the absolute magnitude of the discrepancy between theory and experiment deviate significantly from the values for hydrogen ions shown in Fig. 13. To understand the deviation, we proceed as in Sec. 4.1 by plotting in Fig. 15 the experimental values of Ω^2/Ω^2_B as a function of energy per nucleon for helium ions and for protons, and the difference between the two averaged curves in Fig. 15 is plotted as points in Fig. 16. As expected, these difference values for helium mainly contain contributions from charge-state fluctuations (lower solid curve), and the atomic correlation term (dot-and-dash curve) only amounts to a small correction. The figure has been discussed in detail in Sec. 4.1.

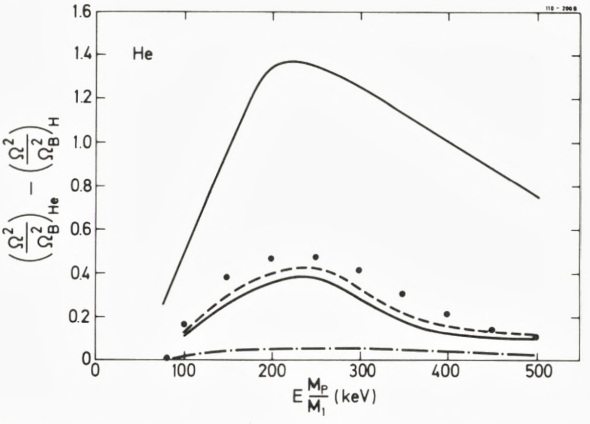

Fig. 16: The deviation from the Z_1^2 scaling of energy straggling for H and He ions in He versus energy per nucleon. The points display the difference between the experimental He and H results in Fig. 15. The contribution from charge-state fluctuations Ω_c^2 (Eqs. (19) and (26)) for He ions, measured in units of Ω_B^2(He), is given by the lower solid curve, whereas the upper solid curve shows the incorrect value of Ω_c^2 calculated previously under the assumption that the stopping cross section for He^+ is equal to that for protons. The difference between the atomic correlation terms (for He given by Eq. (15) times 0.5, cf. II, and zero for H_2) in units of Ω_B^2 for He and H ions is represented by the dot-and-dash curve for an atomic area of $10\pi a_0^2$. When the contribution from charge-state fluctuations is added, the dashed curve results.

4.4 *Molecular Correlation Effects*

In Figs. 17 and 18 are shown the experimental straggling data for hydrogen and helium ions in N_2, O_2, and CO_2. To investigate the molecular correlation effect, we need information on the straggling in targets where the molecules have been dissociated into their constituent atoms. Experimentally, it is extremely difficult to obtain such dissociated targets, and therefore neon was chosen as an atomic reference in the evaluation of molecular correlation effects. According to Bonderup and Hvelplund (1971), the Z_2 dependence of the straggling normalized to the asymptotic Bohr value is very weak when plotted as a function of the reduced variable x, and it is therefore a good approximation to use neon as an atomic reference for N_2, O_2, and CO_2.

In Figs. 19 and 20, the straggling results for the molecular and atomic targets are therefore shown as a function of x. It is evident that the molecular targets cause a consistently higher straggling than the atomic ones, and the difference between the curves may be interpreted as a molecular correlation effect.

For N_2 and O_2 in Figs. 19 and 20, the molecular bunching term Ω_M^2, calculated from the asymptotic formula (17a) with experimental stopping cross sections taken from I, is indicated by arrows. It is seen that both the energy dependence and the absolute value of the correction term are in fairly good agreement with experimental data.

However, the applicability of the asymptotic formula (17a) is questionable since the assumption underlying this expression is far from being fulfilled. This is seen by a comparison of the internuclear distances in nitrogen and oxygen ($d(N_2) = 1.1$ Å and $d(O_2) = 1.21$ Å) with the atomic radius $r_A = 1.65$ Å for an atomic area of $10\pi a_0^2$. Nevertheless, if it is correct that the smaller of the two values in Eq. (17) gives a reasonable estimate of the molecular correlation term Ω_M^2, the asymptotic formula (17a) is, in fact, the appropriate expression for Ω_M^2 in the case of oxygen, and it only overestimated Ω_M^2 for nitrogen by $\sim 10\,\%$.

According to Sigmund (1976), the description of the molecular correlation effect in diatomic molecules can easily be generalized to polyatomic molecular targets, for which the straggling correction per molecule takes on the form

$$\Omega_M^2 = \sum_{i \neq j} \frac{S_i S_j}{2\pi d_{ij}^2} N\Delta R\,, \tag{29}$$

where the sum extends over the constituent atoms $i = 1, 2, \ldots$ of the molecule. This correction term is indicated in Figs. 19 and 20 for CO_2, and again, reasonably good agreement with the experimental results is found.

It should be noticed that for CO_2, which is a linear molecule, the same type of correlation term as that in Eq. (29) is obtained if the somewhat different treatment of correlation effect described in II is used. Generally, for nonlinear polyatomic molecules, Eq. (29) may overestimate the influence of molecular correlations.

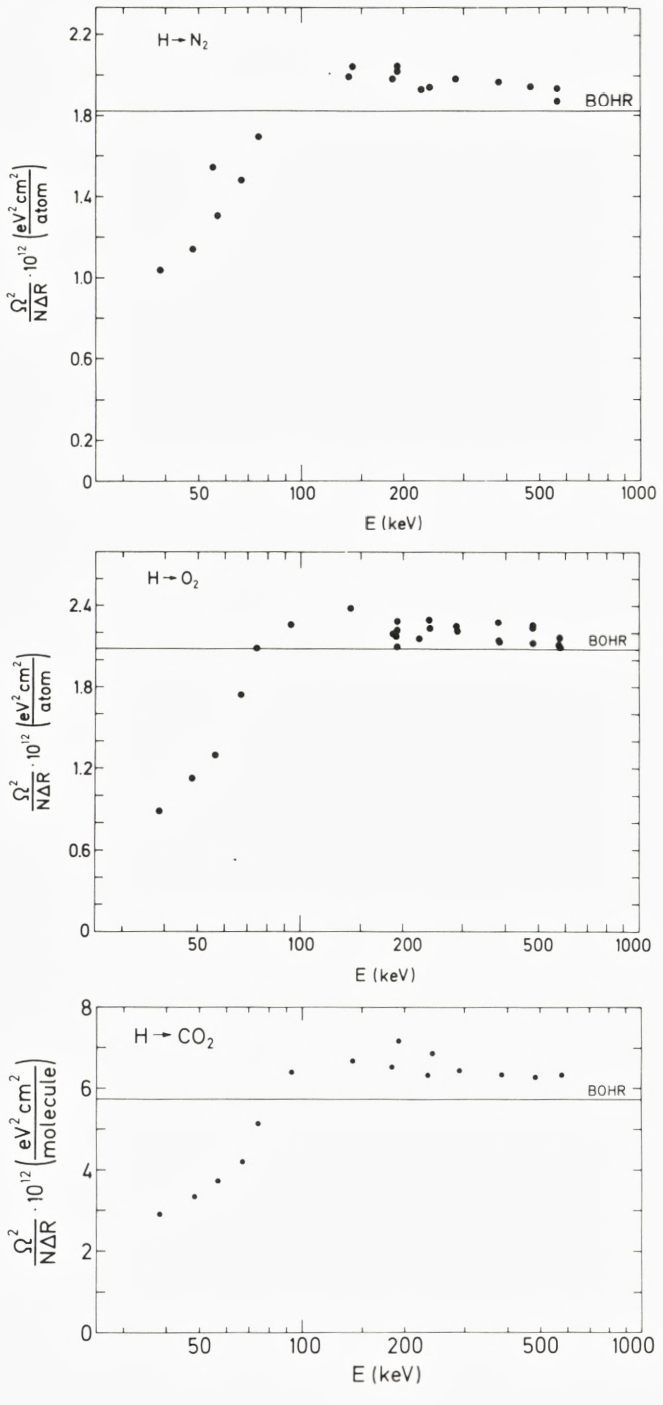

Fig. 17: Experimental straggling data for H ions in N_2, O_2, and CO_2.

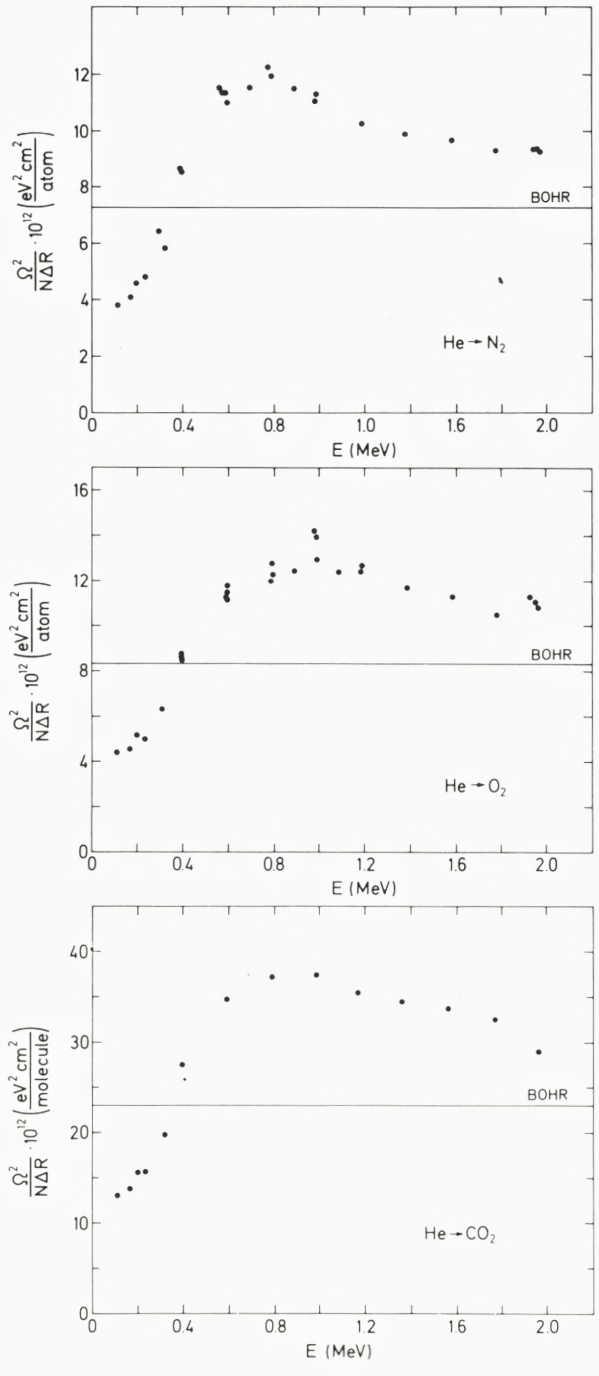

Fig. 18: Experimental energy-straggling data for He ions in N_2, O_2, and CO_2.

Fig. 19: Straggling results for protons in N_2, O_2, and CO_2 from Fig. 17 are compared with straggling results for protons in Ne from Fig. 7. Solid curves drawn through the experimental results are drawn only to guide the eye, whereas the arrows indicate the asymptotic molecular-correlation term Ω_M^2 (Eqs. (17a) and (29)).

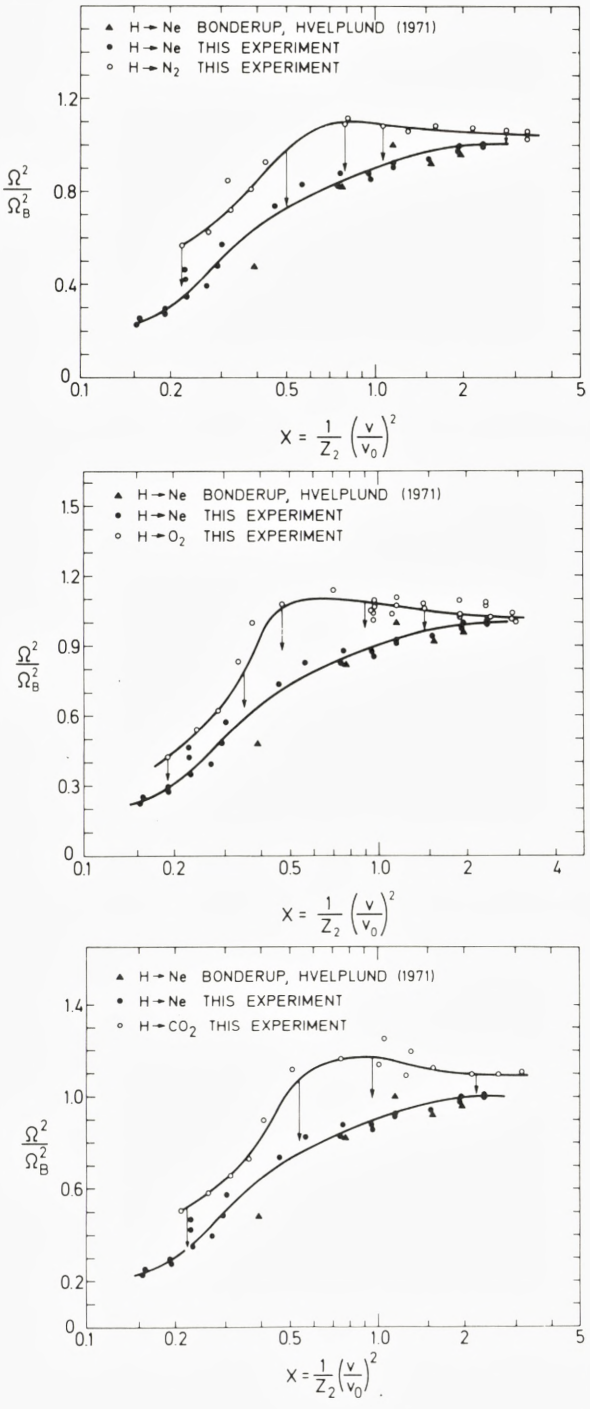

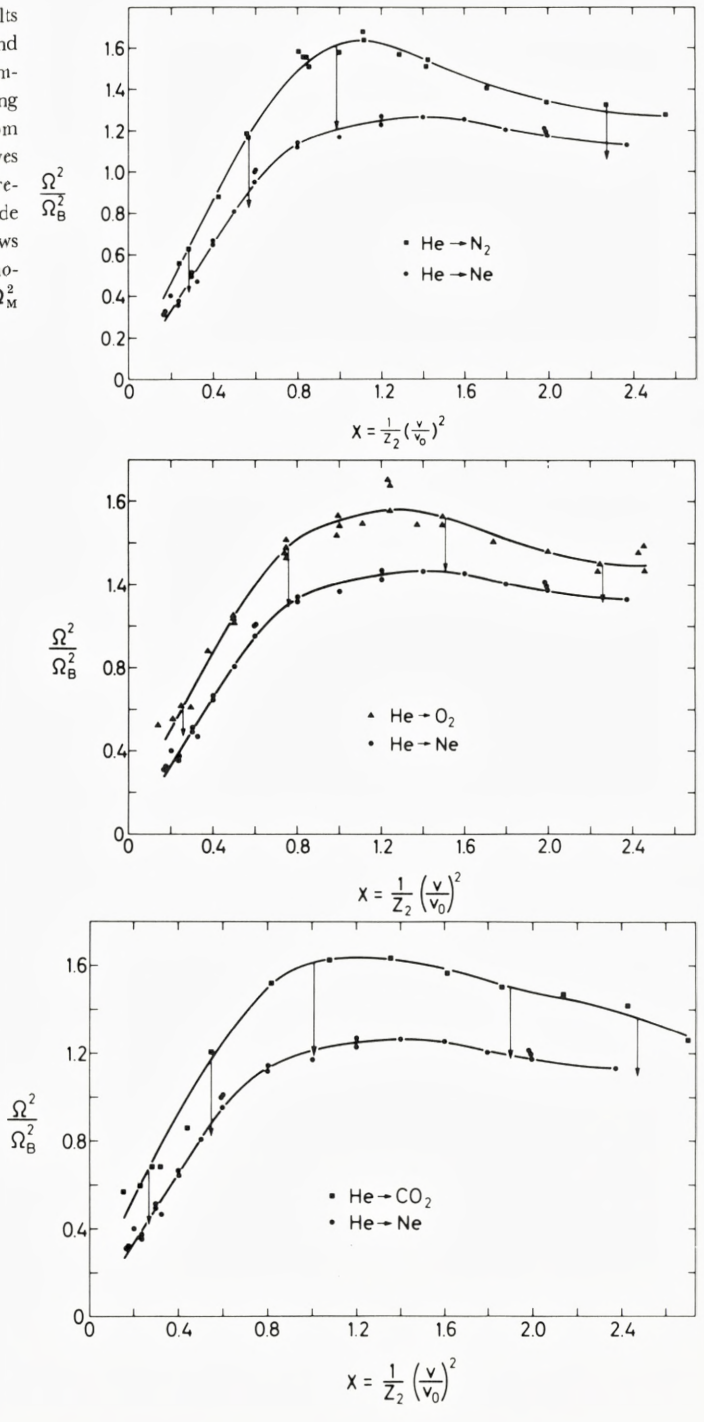

Fig. 20: Straggling results for He ions in N_2, O_2, and CO_2 from Fig. 18 are compared with the straggling results for He ions in Ne from Fig. 8. The solid curves through the experimental results are drawn only to guide the eye, whereas the arrows indicate the asymptotic molecular correlation term Ω_M^2 (Eqs. (17a) and (29)).

4.5 *Straggling in Hydrogen*

The straggling results for hydrogen ions transmitted through a hydrogen target are shown in Fig. 21 together with the results from the asymptotic Fano formula

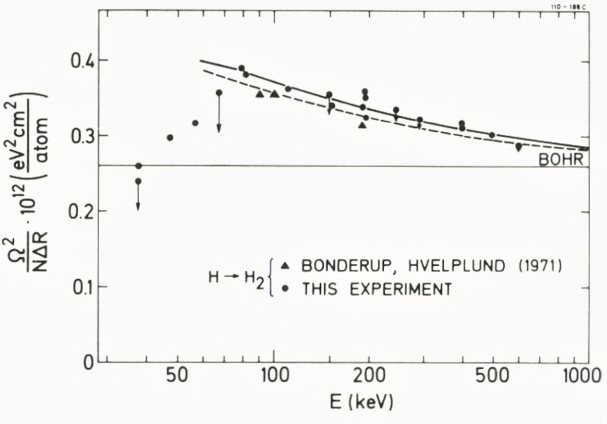

Fig. 22: Experimental energy-straggling results for protons penetrating a H_2 target compared with the asymptotic straggling formulas of Bohr (Eq. (5)) and Fano (Eq. (6)), the latter calculated for molecular (solid curve) and atomic targets (dashed curve). Arrows indicate the molecular correlation term Ω_M^2 given by Eq. (17b).

(6) for molecular (the full-drawn curve) and atomic (the dashed curve) hydrogen. The values of $S(1)$ and I_1 for molecular and atomic hydrogen have been calculated by Zeiss et al. (1977) and Inokuti et al. (1978), respectively, and they are shown in the table below.

	I_1 (eV)	$\frac{1}{Z_2} S(1)$ (eV)
H_2	29.13 eV	22.79 eV
H	24.07 eV	18.13 eV

The difference in I_1 and $S(1)$ reflects the change in electron density and thereby in the oscillator-strength distribution upon molecular formation.

When H_2 molecules are considered as the basic target elements in the straggling calculation, molecular correlation effects caused by two-electron excitations in an H_2 molecule are in principle included in the Fano formula, but as for He not in practice since the I_1 and $S(1)$ values for H_2 only include one-electron excitations. However, according to the discussion in Secs. 4.1 and 4.3, the molecular bunching term Ω_M^2 is small for hydrogen, and the good agreement between the experimental data and formula (6) for energies as low as 80 keV therefore supports the Fano formula.

To indicate that the molecular correlation term Ω_M^2 actually is fairly small

for hydrogen, Ω_M^2 calculated from Eq. (17b) is shown in Fig. 21. Equation (17b) is used since the intermolecular distance is only 0.74 Å and the asymptotic formula (17a) would overestimate Ω_M^2 by a factor of ~ 2.5.

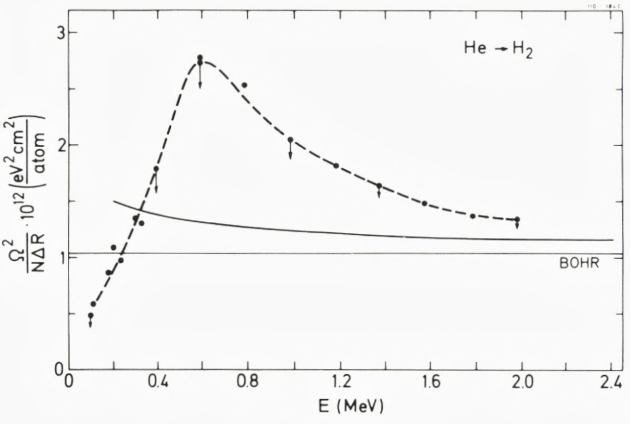

Fig. 22: Experimental energy-straggling results for He ions in H_2 compared with the asymptotic straggling formulas by Bohr (Eq. (5)) and Fano (Eq. (6)). Arrows indicate the molecular correlation term Ω_M^2 given by Eq. (17b).

In Fig. 22, the experimental straggling results for helium ions penetrating hydrogen are compared with the results from the asymptotic Fano formula (6) for molecular hydrogen. A combination of three different effects leads to an increase of the straggling to a factor of as much as 2.6 above the atomic Bohr value. Of the three effects, i.e., (i) the "overshoot" in Eqs. (6) and (11a) caused by the non-vanishing electron velocities, (ii) the molecular correlation effect, and (iii) the charge-state-fluctuation effect, the latter being by far the dominating one for a hydrogen target. This is seen from Fig. 23, where the difference between the averaged helium and hydrogen results in Figs. 21 and 22 in units of Ω_B^2 is compared to the contribution from the different effects. In the calculation of Ω_C^2 from Eqs. (19) and (26), the capture and loss cross sections by Hvelplund et al. (1976, 1980) have been applied. The agreement between the experimental results and the dot-and-dash curve, which is the sum of the contributions from Ω_C^2, Ω_M^2, and Ω_F^2 (Eq. (6)), is reasonable but certainly not as good as for the helium case in Fig. 16.

4.6 *Connection to Other Measurements*

As argued in II, the straggling of light, swift ions may be theoretically simpler in a solid than in a gas. In a solid, the effective atomic diameter $2r_A \sim 3.3$ Å is of the order of the interatomic distance and the fluctations in the number of ion-atom encounters, and thus the atomic correlation term Ω_A^2 will be small as com-

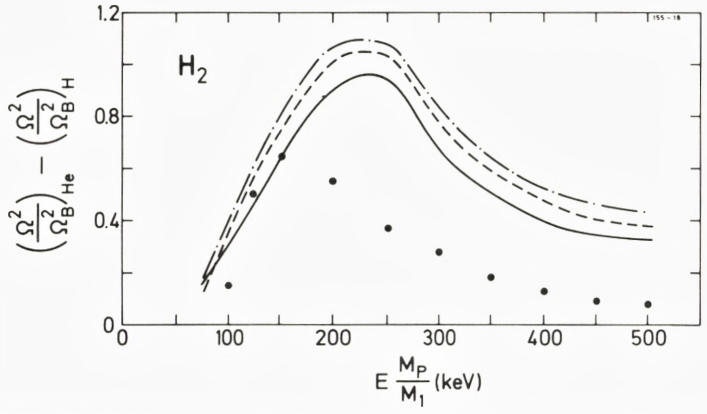

Fig. 23: The deviation from the Z_1^2 scaling of energy straggling for H and He ions in H_2 versus energy per nucleon. The points display the difference between the experimental H_2 results in Figs. 21 and 22. The contribution from charge-state fluctuations Ω_C^2 (Eqs. (19) and (26) for He ions measured in units of Ω_B^2(He) is given by the solid curve. When the contribution from molecular correlation effects Ω_M^2 (Eq. (17b) is added, the dashed curve results. When finally the contribution from the Fano formula (Eq. (6)) is added, the dot-and-dash curve results.

pared to that in a gas of the same area density $N\Delta R$. Similarly, charge-state fluctuations in a gas, resulting in the straggling term Ω_C^2, is for a solid reduced to a significantly smaller fluctuation of the screening cloud travelling with the ion. Thus we would expect the straggling in a metal to agree approximately with the electron-gas results, an expectation which is actually borne out by recent measurements by Heine et al. (1979) on aluminium (Fig. 6 in II).

Generally, however, straggling data for hydrogen and helium ions in solids deviate from the theoretical electron-gas estimates, and measurements on the same target by different groups may even deviate by as much as a factor of two (Fig. 7 in II). One of the reasons why it is so difficult to deduce any systematics from straggling measurements in solids is probably that the target inhomogeneities such as, e.g., non-uniform film thickness and texture effects tend to increase the straggling in an uncontrollable way. It is worthwhile to point out, however, that in many applications of straggling results to ion-beam analysis of solids, the difficulties, which hamper accurate, reliable, and reproducible measurements on thin solid films, often are reduced, and thus a precise knowledge of the basic straggling term Ω_{Ls}^2 caused by fluctuations in electron excitation is still of great importance. Experimentally, such information can be obtained for solids only if a proper check and/or correction for foil inhomogeneities is performed. Unfortunately, only very few experiments on solids have been made with proper control of the target conditions, and we shall abstain from a further discussion of straggling

data for light ions in solids and concentrate upon the straggling data for gaseous targets.

Hvelplund (1968, 1971, 1975) and Bonderup and Hvelplund (1971) performed an extensive investigation of energy straggling suffered by keV ions penetrating gas targets. A comparison with Hvelplund's straggling results for hydrogen ions transmitted through H_2, He, Ne, Ar, Kr, and for helium ions penetrating He and Ne is made in the respective figures of this work. For the cases of $H \rightarrow H_2$, He, Ne, Kr, Hvelplund's straggling data agree with the present ones within the uncertainties, while in the case of $H \rightarrow Ar$ and $He \rightarrow He$, Ne at the highest energies, the two sets of data deviate by approximately 20 %. The reason for this discrepancy is not understood, but it may be mentioned that also the stopping-power data in Ar by Bonderup and Hvelplund appear to be low (see I).

Mason et al. (1966), Ramirez et al. (1969), and Haque and Hora (1972) have measured straggling for protons and α particles in gases. In these experiments, the mean energy loss is considerable compared to the initial energy, and a comparison with the present measurements becomes difficult. (If $\overline{\Delta E}$ is comparable to E_i, the measured straggling $\Omega^2/N\Delta R$ will be larger than that for negligible energy loss provided the stopping power is a decreasing function of energy, Tschalär (1968).) An exception to the above situation is the $He \rightarrow He$ data by Ramirez et al. (1969), where $\Delta E/E_i$ is only ~ 18 %. For energies of $1.5 \lesssim E_{He} \lesssim 3.5$ MeV, Ramirez et al. (1969) found that Ω/Ω_B is approximately a constant equal to 2.5, decreasing slowly with increasing energy. This result deviates drastically from the present findings shown in Fig. 14.

Cameron et al. (1977) have measured straggling for low-energy α particles in helium. Comparing their data for the lowest energy losses with those shown in Fig. 14, good agreement is found for energies below 400 keV, while for higher energies, the discrepancy increases with energy, resulting in a difference of a factor of 3 in Ω^2 for $E = 1070$ keV.

Concerning the above discrepancies in the helium data, it might be mentioned that in the experiments by both Cameron et al. and Ramirez et al., the energy spread of the incident α-particle beam is not negligible as compared to that resulting from the penetration of the helium gas, and this might obscure the straggling results.

Recently, there has been a growing interest in straggling for heavy ions because of its importance for many heavy-ion-accelerator experiments. Efken et al. (1975) have measured energy-loss straggling of N, Ne, and Ar ions in He, N_2, SF_6, and Ar-gas targets and in carbon foils at energies of 5–15 MeV. All these measurements were performed in the thin-absorber limit $\overline{\Delta E}/E_i \lesssim 0.1$. For monatomic targets, the measured straggling was significantly higher (1.5–2.5) than the straggling due to fluctuations in electron excitations, calculated from

the Vavilov theory (Vavilov (1957)). Efken et al. attributed this discrepancy to the straggling contribution Ω_C^2 caused by charge-state fluctuations and, using either formula (19) or Monte-Carlo calculations to predict Ω_C^2, they were able to explain their experimental findings qualitatively.

However, their measurements belong to the velocity-proportional stopping region $v \lesssim v_0 Z_1^{2/3}$, and thus the Vavilov theory is not applicable since the assumption underlying the Vavilov theory and the Bohr formula (Eq. 5) is similar, i.e., all of the target electrons contribute to the straggling as free electrons at rest, and the cross section is given by the Thomson formula (Eq. 4). In the low-velocity region, the straggling due to fluctuations in electron excitations is small as mentioned in Sec. I and discussed in detail in II. The straggling results mainly from the statistical distribution in impact parameters in the ion-atom collisions, and within the Firsov model, it is given by Eq. (16).

In Fig. 24, the experimental straggling data for heavier ions at low and medium velocities by Efken et al. (1975), Hvelplund (1971), Andersen et al. (1978), Sofield et al. (1978), and Cowern et al. (1979) are compared with the Hvelplund-Firsov low-velocity straggling formula (16) and the high-energy Bohr formula (5). When the straggling in Bohr units is plotted versus the parameter $[(Z_1+Z_2)^{8/3}/(Z_1^2 Z_2)]\left(\frac{v}{v_0}\right)^2$, formula (16) leads to a universal straight line.

From Fig. 24 it is seen that the straggling data by Efken et al. (1975) on atomic targets, and also the molecular results, when corrected for the molecular-correction term Ω_M^2, agree with the general trend of the straggling results by Hvelplund (1971) and Andersen et al. (1978) and with Eq. (17) to within a

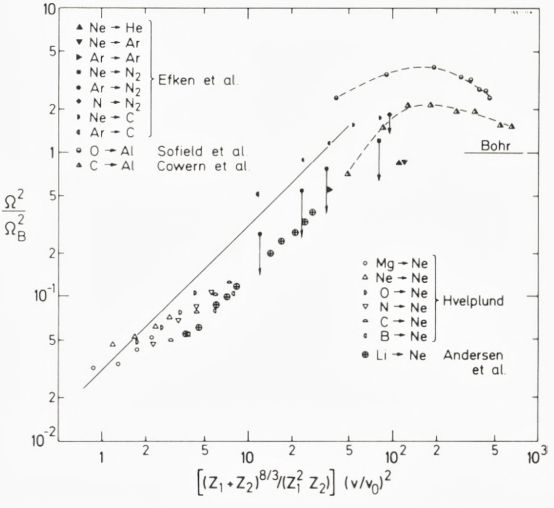

Fig. 24: The experimental straggling results for heavy ions at low and medium velocities by Efken et al. (1975), Hvelplund (1971), Andersen et al. (1978), Sofield et al. (1978), and Cowern et al. (1979) are compared with the Hvelplund-Firsov low-velocity straggling formula (16), and the high-energy Bohr formula (5). The dashed curves through the data of Sofield et al. and Cowern et al. are made only to guide the eye, whereas the arrows indicate the molecular correlation term Ω_M^2.

factor of 1–2. It therefore seems unneccessary to incorporate the straggling term Ω_C^2 to explain the experimental gas data by Efken et al.

In Fig. 24 are also shown the straggling results of Efken et al. for Ne and Ar ions on thin carbon foils. These solid-target results are systematically higher than the results on atomic gas targets. According to the authors, this may be due to the influence of foil inhomogeneities.

First, in Fig. 24 are shown the experimental straggling results of the Harwell group [Sofield et al. (1978) and Cowern et al. (1979)] for nearly fully stripped ^{16}O and ^{12}C ions penetrating aluminum foils. For the lowest energies, the experimental results again agree with Eq. (17) to within a factor of 1–2. At the highest energies, the data are significantly higher than the predictions based on the Livingstone-Bethe formula (Livingstone and Bethe (1937)), which is a semi-empirical version of the perturbation formulas, Eqs. (6) and (7), with the atomic quantities expressed in terms of ionization potentials and effective charges for the various electronic shells. The deviations from the Livingstone-Bethe formula was attributed to the straggling contribution Ω_C^2 from charge-state fluctuations, and on the assumption that Ω_C^2 is given by Eq. (19) and that the partial stopping cross sections can be written as $S_q = q^2 S_p$, experimental values of the electron-capture and -loss cross sections σ_{56} and σ_{65} were determined for ^{12}C.

However, the results may be vitiated by large uncertainties. First, the assumption that the stopping-power scales as the average square of the charge state may lead to an overestimate of the influence of charge-exchange straggling Ω_C^2 even though one may expect the error to be smaller than in the helium-ion case discussed above. Also the applicability of the Bethe-Livingstone perturbation formula might be questionable since the parameter $\kappa_B = 2Z_1 v_0/v$ is of the order of unity. A better way to obtain information on Ω_C^2 would be to compare the ^{12}C results with experimental-straggling results for a lighter ion, which is in a fixed charge state, i.e., to use a method similar to that used in Sec. 4.1.

Second, the measurements may be obscured by straggling contributions from foil inhomogeneities on a microscopic scale. Such effects were carefully checked by the Harwell group by means of a 25-μm diameter proton beam and a 2×0.1-μm Tallystep profiler, and it was concluded that thickness variations over distances larger than the lateral resolution of 2×10^5 Å and 2×10^4 Å for the methods contribute to the straggling by less than 10 %. It is, however, noteworthy that the energy dependence of the straggling is nearly identical to the energy dependence of the stopping power, which is exactly what is expected for a contribution $\Omega^2_{\Delta t}$ from thickness variations since $\Omega^2_{\Delta t} = (dE/dx)^2 \Delta t^2$, where Δt is the standard deviation of the foil-thickness distribution. It may therefore still be worthwhile to check for foil-inhomogeneity effects by comparing the straggling in the foils for different light ions such as protons, α particles, and lithium ions, for which

the influence of charge-state fluctuations is negligible. The applicability of this method, which has a high lateral resolution, has been demonstrated by the Oak Ridge group (see II for further details).

Finally, in our opinion, the ultimate test of the influence of charge-exchange straggling for heavy ions would be obtained from measurements with ^{12}C in a gas target since the electron-capture and -loss cross sections are either known or can be measured separately, and the problems with target inhomogeneities disappear.

Acknowledgements

The authors are indebted to J. U. Andersen, E. Bonderup, M. Inokuti, J. Lindhard, and P. Sigmund for their continuous interest in the present work and for the help and guidance received from them in numerous discussions. The assistance extended to us from the technical stoff, particularly V. Toft, is gratefully acknowledged. Finally, we wish to thank Alice Grandjean for her competent assistance in the preparation of the manuscript for the present article.

References

H. H. Andersen, F. Besenbacher, and H. Knudsen, Nucl. Instrum. Methods *149* (1978) 121.

H. H. Andersen and J. F. Ziegler, *Hydrogen Stopping Powers and Ranges in All Elements* (Pergamon, New York, 1977).

A. A. Bednyakov, U. V. Bulgakov, V. S. Nikolaev, V. P. Sobakin, and V. L. Chernov, Phys. Letters *62A* (1977) 183.

F. Besenbacher, Thesis (University of Aarhus, 1977) (unpublished).

F. Besenbacher, H. H. Andersen, P. Hvelplund, and H. Knudsen, Kgl. Danske Vidensk. Selsk., Mat.-Fys. Medd. *40*, No 3 (1979) (I).

F. Besenbacher, J. U. Andersen, and E. Bonderup, Nucl. Instrum. Methods *168* (1980) 1 (II).

F. Besenbacher, J. Heinemeier, P. Hvelplund, and H. Knudsen, Phys. Letters *61A* (1977) 15.

N. Bohr. Kgl. Danske Vidensk. Selsk., Mat.-Fys. Medd. *18*, No 8 (1948).

E. Bonderup, Kgl. Danske Vidensk. Selsk., Mat.-Fys. Medd. *35*, No 17 (1967).

E. Bonderup and P. Hvelplund, Phys. Rev. A *4* (1971) 562.

J. M. Cameron, R. H. McCamis. G. A. Miller, G. A. Moss, G. Roy, and A. W. Stetz, Nucl. Instrum. Methods *145* (1977) 405.

W. K. Chu, Phys. Rev. *A 13* (1976) 2057.

J. Cuevas, M. Garcia-Munoz, P. Torres, and S. K. Allison, Phys. Rev. A *135* (1964) 335.

N. E. B. Cowern, C. J. Sofield, J. M. Freeman, and J. P. Mason, Phys. Rev. A *19* (1979) 111.

J. L. Dehmer, M. Inokuti, and R. P. Saxon, Phys. Rev. A *12* (1975) 102.

B. Efken, D. Hahn, D. Hilscher, and G. Wüstefeld, Nucl. Instrum. Methods *129* (1975) 219.

U. Fano, Ann. Rev. Nucl. Sci. *13* (1963) 1.

O. B. Firsov, Zh. Eksp. Teor. Fiz. *36* (1959) 1517 [Engl. transl. Sov. Phys. JETP *9* (1959) 1076].

A. K. M. M. Haque and R. M. Hora, Nucl. Instrum. Methods *104* (1972) 77.

P. Hvelplund, Thesis (University of Aarhus, 1968) (unpublished).

P. Hvelplund, Kgl. Danske Vidensk. Selsk., Mat.-Fys. Medd. *38*, No 4 (1971).

P. Hvelplund, Phys. Rev. A *11* (1975) 1921.

P. Hvelplund et al. (1980) (private communication).

P. Hvelplund, J. Heinemeier, E. Horsdal Pedersen, and F. R. Simpson, J. Phys. B: Atom. Molec. Phys. *9* (1976) 4911.

M. Inokuti, T. Baer, and J. L. Dehmer, Phys. Rev. A *17* (1978) 1229.

L. Landau, J. Phys. USSR *8* (1944) 201.

J. Lindhard and M. Scharff, Kgl. Danske Vidensk. Selsk., Mat.-Fys. Medd. *27*, No 15 (1953).

J. Lindhard and A. Winther, Kgl. Danske Vidensk. Selsk. Mat. Fys. Medd. *34*, No. 4 (1964).

J. Lindhard, V. Nielsen, and M. Scharff, Kgl. Danske Vidensk. Selsk. Mat.-Fys. Medd. *35*, No. 10 (1968).

M. S. Livingstone and H. A. Bethe, Rev. Mod. Phys. *9* (1937) 245.

D. L. Mason, R. M. Prior, and A. R. Quinton, Nucl. Instrum. Methods *45* (1966) 41.

L. I. Pivovar, V. M. Tubaev, and M. T. Novikov, Zh. Eksp. Teor. Fiz. *41* (1961) 26; ibid. *42* (1962) 1490 [Engl. transl. Sov. Phys. JETP *14* (1962) 20; ibid. *15* (1962) 31].

J. J. Ramirez, R. M. Prior, J. B. Swint, A. R. Quinton, and R. A. Blue, Phys. Rev. *179* (1969) 310.

H. Schmidt-Böcking and H. Herming, Z. Phys. *A286* (1978) 253.

P. Sigmund, Phys. Rev. A *14* (1976) 996.

P. Sigmund, Kgl. Danske Vidensk. Selsk. Mat. Fys. Medd. *40*, No 5 (1978).

C. J. Sofield, N. E. B. Cowern, R. J. Petty, J. M. Freeman, and J. P. Mason, Phys. Rev. A *17*, 859 (1978).

C. Tschalär, Nucl. Instrum. Methods *61* (1968) 141; ibid. *64* (1968) 237.

P. V. Vavilov, Zh. Eksp. Teor. Fiz. *32* (1957) 920 [Engl. transl. Sov. Phys. JETP *4* (1957) 749].
O. Vollmer, Nucl. Instrum. Methods *121* (1974) *373*.
E. J. Williams, Proc. Roy. Soc. A *125* (1929) 420; ibid. A *130* (1931) 328.
J. F. Ziegler, *Helium Stopping Powers and Ranges in All Elements* (Pergamon, New York, 1978).
G. D. Zeiss, W. J. Meath, J. C. F. MacDonald, and D. J. Dawson, Radiat. Research *70* (1977) 284.

Indleveret til Selskabet november 1980.
Færdig fra trykkeriet august 1981.